Molecular Therapy
Original Article

Rapid and Complete Reversal of Sensory Ataxia by Gene Therapy in a Novel Model of Friedreich Ataxia

Françoise Piguet,[1,2,3,4,5] Charline de Montigny,[1,2,3,4,5] Nadège Vaucamps,[1,2,3,4] Laurence Reutenauer,[1,2,3,4] Aurélie Eisenmann,[1,2,3,4] and Hélène Puccio[1,2,3,4]

[1]Institut de Génétique et de Biologie Moléculaire et Cellulaire (IGBMC), 67404 Illkirch, France; [2]Institut National de la Santé et de la Recherche Médicale, U1258, 67404 Illkirch, France; [3]Centre National de la Recherche Scientifique, UMR7104, 67404 Illkirch, France; [4]Université de Strasbourg, 67000 Strasbourg, France

Friedreich ataxia (FA) is a rare mitochondrial disease characterized by sensory and spinocerebellar ataxia, hypertrophic cardiomyopathy, and diabetes, for which there is no treatment. FA is caused by reduced levels of frataxin (FXN), an essential mitochondrial protein involved in the biosynthesis of iron-sulfur (Fe-S) clusters. Despite significant progress in recent years, to date, there are no good models to explore and test therapeutic approaches to stop or reverse the ganglionopathy and the sensory neuropathy associated to frataxin deficiency. Here, we report a new conditional mouse model with complete frataxin deletion in parvalbumin-positive cells that recapitulate the sensory ataxia and neuropathy associated to FA, albeit with a more rapid and severe course. Interestingly, although fully dysfunctional, proprioceptive neurons can survive for many weeks without frataxin. Furthermore, we demonstrate that post-symptomatic delivery of frataxin-expressing AAV allows for rapid and complete rescue of the sensory neuropathy associated with frataxin deficiency, thus establishing the pre-clinical proof of concept for the potential of gene therapy in treating FA neuropathy.

INTRODUCTION

Friedreich ataxia (FA), the most prevalent cause of recessive hereditary ataxia, is an early-onset neurodegenerative disease characterized by progressive spinocerebellar ataxia, severe proprioceptive sensory loss, cardiomyopathy, and increase in incidence of diabetes mellitus.[1,2] Both the CNS and the peripheral nervous system (PNS) are primarily affected. Proprioceptive sensory loss in the PNS is an early feature of the disease, while the cerebellar and spinocerebellar involvement contribute to the progression of the disease.[2] The neurological symptoms are a consequence of degeneration of the large sensory neurons of the dorsal root ganglia (DRGs) and their axons, of the spinocerebellar tracts,[2–4] as well as lesions in the dentate nuclei of the cerebellum and Purkinje cells.[3,5] In addition, more recent studies provide evidence of cerebral involvement.[6] FA is associated with a shortened lifespan, with cardiac dysfunction the main cause of mortality.[7] The disease is caused by a $(GAA)_n$ expansion within the first intron of the frataxin gene (*FXN*).[8] The mutation results in heterochromatin formation[9] leading to reduced expression of frataxin (FXN), a highly conserved mitochondrial protein, involved in iron-sulfur biogenesis.[10,11] To date, there is no efficient treatment for FA.

Replenishment of frataxin either through epigenetic drugs, protein replacement, or gene therapy would be the optimal therapy for FA. Previously, we established a proof of concept for a gene therapy approach using adeno-associated virus (AAV)-expressing frataxin (AAV-FXN) to prevent and rapidly reverse the cardiomyopathy associated with FA.[12] Our study clearly demonstrated that dysfunctioning frataxin-deficient cardiomyocytes were still viable after the onset of heart failure and that their phenotype could be reversed. However, one critical question in the field is whether the ganglionopathy and sensory peripheral neuropathy reflect irreversible cell death or whether it is a consequence of neuronal dysfunction that could potentially be reversible. To address this question and with the aim of developing a gene therapy approach to tackle the neuropathology associated with FA, we developed a new neuronal conditional model of the disease. Although several mouse models of FA have already been generated, none are suited for testing gene therapy approaches for the primary sensory ataxia associated with FA. Indeed, while the GAA expansion-based models (KIKO, YG8, and YG22 models) are good models to assess the epigenetics consequence of the GAA expansion and early pathophysiological consequences of frataxin deficiency, they failed to display a robust behavioral phenotype.[13–18] Other models have been generated based on the Cre-Lox technology to knockout frataxin in specific neuronal cells; however, these models are too severe and non-specific, such as the neuronal-specific enolase (NSE) model,[19] or develop a later onset pathology and have simultaneously DRG and cerebellar ataxia with severe granule cell

Received 8 March 2018; accepted 5 May 2018;
https://doi.org/10.1016/j.ymthe.2018.05.006.

[5]These authors contributed equally to this work.

Correspondence: Hélène Puccio, IGBMC, 1 rue Laurent Fries, 67404 Illkirch, France.
E-mail: hpuccio@igbmc.fr

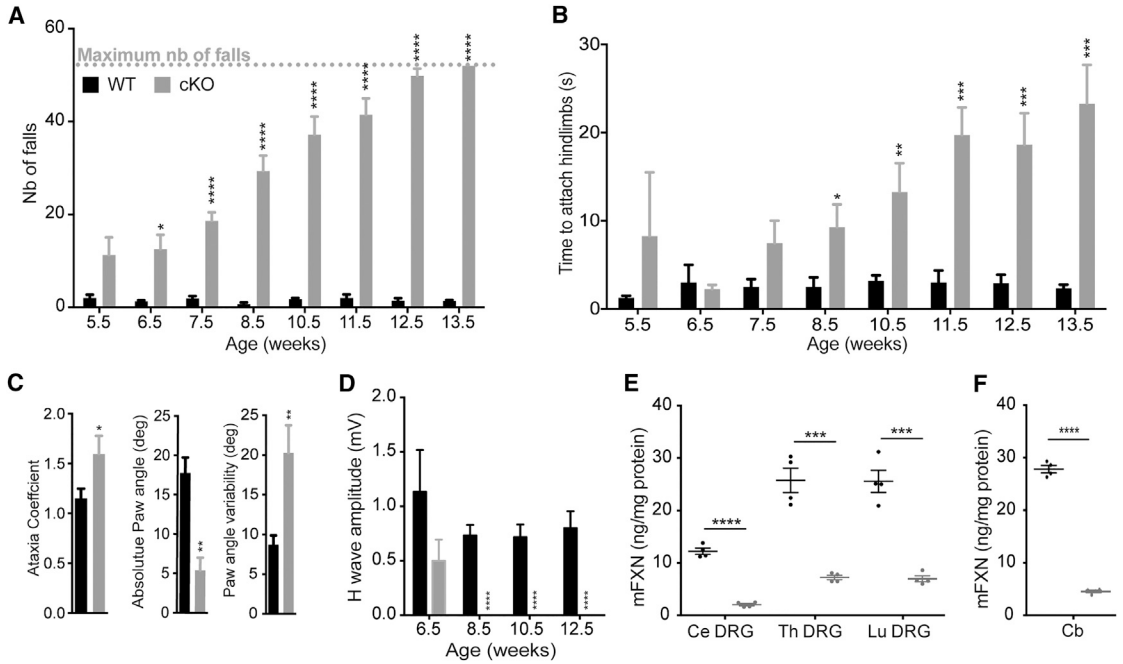

Figure 1. Impaired Behavior and Specific Loss of Sensory Wave in *Pvalb* cKO Mice Associated with Large Frataxin Depletion in DRG and Cerebellum

(A) Notched-bar test analysis, number of footfalls is represented; n = 10 WT and n = 11 *Pvalb* cKO. (B) Hanging-wire test analysis, time needed to attach hindlimbs to the string is represented; n = 10 WT and n = 11 *Pvalb* cKO. (C) Ataxia coefficient, measurement of absolute paw angle and paw angle variability after 5 s of walk on the DigitGait apparatus at 13.5 weeks of age; n = 6 WT and n = 5 *Pvalb* cKO. (D) Amplitudes of somatosensory wave (H-wave) were recorded after plantar sciatic nerve stimulation; n = 6 WT and n = 7 *Pvalb* cKO. (E and F) Mouse Frataxin expression levels evaluated by ELISA on cervical, thoracic, and lumbar DRG (E) and on cerebellum (F), in WT and *Pvalb* cKO mice at 7.5 weeks of age. n = 4. Data are represented as mean ± SEM. *p < 0.05; **p < 0.01; ***p < 0.001; ****p < 0.0001.

degeneration.[20] We thus generated a new conditional model using the $Pvalb^{tm1(Cre)Arbr/J}$ mouse line[21] to more specifically target the proprioceptive neurons. The $Pvalb^{tm1(Cre)Arbr/J}$ knockin allele has the endogenous parvalbumin promoter and enhancer elements directing Cre recombinase expression in cells expressing parvalbumin, such as proprioceptive afferent sensory neurons in the DRG, cerebellar Purkinje cell, and deep nuclei, as well as interneurons in the brain.[21]

The newly generated *Pvalb-Cre* conditional knockout (cKO) model recapitulated features of FA neuropathophysiology, in particular a ganglionopathy with sensory axonopathy, albeit with a more rapid and severe course of the disease. In addition, a cerebellar ataxia and cerebral involvement occur, but after the onset of the PNS pathology. Intravenous delivery of AAV-FXN fully prevented the onset of peripheral sensory neuropathy. Moreover, combined intravenous and intracerebral delivery AAV-FXN, after the onset of behavioral impairment, was able to reverse the phenotype of these mice at the behavioral, physiological, and cellular levels within a few days. Our results strongly demonstrate that frataxin-deficient proprioceptive neurons with severe phenotype survive for several weeks and can be rapidly and completely rescued by gene therapy in the mouse model. Thus, this study establishes the pre-clinical proof of concept for the potential of gene therapy in treating FA sensory neuropathy.

RESULTS

Pvalb cKO Mimics Neuropathophysiology Occurring in FA Patients

To induce frataxin deletion in parvalbumin-positive neurons (including the proprioceptive neurons of DRG, cerebellar deep nuclei, and Purkinje cells), we bred mice homozygous for the conditional frataxin allele ($Fxn^{L3/L3}$) with mice heterozygous for the frataxin allele carrying the *Pvalb-Cre* transgene ($Fxn^{+/L-}$; $Pvalb^{tm1(Cre)Arbr/J}$). Animals were born according to Mendelian ratio indicating no substantial embryonic lethality and displayed a normal growth until 21.5 weeks (Figure S1A). Loss of coordination in *Pvalb* cKO mice was evaluated weekly from 5.5 weeks until 13.5 weeks. *Pvalb* cKO mice developed a rapidly progressive movement disorder characterized by gait abnormality as early as 6.5 weeks of age on the notched-bar test (Figure 1A) and general coordination defects measured at 8.5 weeks of age on the wire-hanging test (Figure 1B) and on the rotarod (Figure S1B). The loss of coordination progressed over time, and *Pvalb* cKO mice showed a complete incapacity at the notched bar by 13.5 weeks of age (Figure 1A). Open field analysis did not reveal any change in general locomotor activity (Figures S1C and S1D). Digit gait analysis performed on a sub-cohort of mice at 13.5 weeks of age confirmed the ataxic gait in *Pvalb* cKO animals, with a significant increase in the ataxic coefficient, a decrease in absolute hindpaw angle, and an increase in paw angle variability (Figure 1C). On electromyographic measurements, motor-evoked

potential measurements in plantar muscle were normal (Figure S1E). In contrast, after somatosensory stimulation of the sciatic nerve, the H-wave response (sensorimotor reflex) was significantly affected at 8.5 weeks of age with a complete loss ($p < 0.0001$) (Figure 1D; Table S1), indicating that the large myelinated proprioceptive sensory neurons or their afferents are functionally defective. As a general observation, *Pvalb* cKO mice develop tremors after 8.5 weeks of age, worsening over time, and died prematurely around 21 weeks of age due to epileptic seizures. The expression of the Cre recombinase in the Purkinje cells at p40, as well as more widely throughout the cortex at 21.5 weeks, most likely contributes to the phenotype of the mice, in particular the tremors and the epileptic seizures (Figure S2; see Supplemental Results).

In agreement with the expression pattern of the *Pvalb-Cre* transgene, frataxin depletion was observed in the DRG, brain, cerebellum, and spinal cord by western blot (Figures S1F and S1G). By ELISA assay, a very strong reduction of frataxin (72%–83% reduction) was seen in the DRG of the *Pvalb* cKO compared to control (Figure 1E; Table S2), despite the fact that the proprioceptive neurons (i.e., the ones expressing the Cre recombinase) represent only 7.5% of the total cells of the DRG.[22,23] Considering that the *Pvalb* cKO are constitutive heterozygotes for the frataxin locus ($Fxn^{L3/L-}$), this demonstrates that proprioceptive neurons express 44%–66% of the total frataxin of the DRG (Table S3; Supplemental Results). Interestingly, lumbar DRG express twice as much frataxin than the cervical DRG (Figure 1E), while no clear differences was observed in different sections of the spinal cord (Figure S1G). Similarly, in the cerebellum, the Purkinje cell and the deep gray nuclei express 67% of the total frataxin expression of the cerebellum (Figure 1F; Table S3).

To determine the pathological changes associated with frataxin deficiency, histological analysis was performed on both DRG and cerebellum. The main pathological feature in the DRG was the presence of vacuoles in ~1.5% of neurons at 7.5 weeks in *Pvalb* cKO ($p = 0.0429$) (Figure 2A). No neuronal loss in the DRG was observed at 7.5 weeks of age (Figure 2B), demonstrating that the loss of somatosensory response is not a consequence of neuronal loss. At 10.5 weeks of age, although not statistically significant, a trend of 10%–15% neuronal loss in the lumbar level was observed, a tendency not further exacerbated with time (Figure 2B). Neurofilament 200 staining, a marker of proprioceptive and mechanoreceptive neurons, shows a reduction of ~30% of large myelinated neurons at 21.5 weeks in *Pvalb* cKO (Figures S3A and S3B). No neuronal loss in the cervical or thoracic DRG was observed at any time despite frataxin deletion demonstrating some specificity toward lumbar DRG (Figure S3C). In the cerebellum, abnormal localization and loss of Purkinje cells was also observed starting at 10.5 weeks of age (Figures 2C and 2D).

To further determine the pathological changes associated with the specific loss of sensory wave, ultrastructural analysis was performed on both DRG and the sciatic nerve, a mixed sensory and motor nerve. Ultrastructural analysis of DRG neurons presenting vacuoles at 7.5 weeks of age (Figure 2A, arrows) revealed signs of mitochondrial and cell degeneration. Typical features of different stages of mitophagy were observed: mitochondria starting to degenerate (Figure 2E, arrows 1), large vacuoles with membrane invagination and cytoplasmic material inside (Figure 2E, arrows 2), complete degeneration of the cell with endoplasmic reticulum (ER) dilation (Figure 2E, arrows 3). At 3.5 weeks of age, sciatic nerves of *Pvalb* cKO already displayed signs of neuropathy with degeneration affecting small caliber myelinated fibers and inner swelling tongue (Figure 2F). Such abnormalities became more frequent and severe with age. At 5.5 weeks, degenerating mitochondria were noted (Figure 2F), while by 17.5 weeks of age, clear signs of axonal loss as well as axonal shrinkage were observed, with the frequent presence of myelin debris (Figure 2F). In agreement with the lack of pathology in the thoracic and cervical DRG, analysis of radial and median nerve at 18.5 weeks did not show any abnormalities (Figure S3D).

The molecular events following frataxin depletion are iron-sulfur (Fe-S) cluster protein deficits and cellular iron dysregulation.[19,24] We initially measured SDH activity on lumbar DRG and cerebellum protein lysates by spectrophotometry; however, no difference between wild-type (WT) and *Pvalb* KO was observed (Figures S4A and S4B). Similarly, western blot analysis of the lipoic acid bound to pyruvate dehydrogenase (PDH) and α-ketoglutarate dehydrogenase (KGDH) complexes did not reveal any differences, suggesting that the Fe_4S_4-dependent lipoic acid synthase was not affected (Figures S4C and S4D). However, we hypothesized that the absence of detectable Fe-S cluster protein deficit in whole lysate of DRG and cerebellum might be a consequence of signal dilution, as proprioceptive neurons represent only 7.5% of the total cells of the DRG and Purkinje cell represents a minority of cerebellar cells (1 Purkinje cell for 778 granule neurons[25]). SDH activity was determined by histoenzymatic staining on cryostat sections of lumbar DRG and cerebellum (Figures 3A–3C). In lumbar DRG sections of *Pvalb* cKO animals, large SDH-negative neurons were observed at 8.5 weeks of age (Figure 3A, zoom). Quantification of SDH staining in DRG demonstrated a significant increase in the number of negative SDH neurons in *Pvalb* cKO animals compared to WT as early as 5.5 weeks of age (Figures 1B and S4E). Similarly, in the cerebellum, faint SDH staining was observed in *Pvalb* cKO Purkinje cells compared to control animals at 13.5 weeks of age (Figure 3C). At 18.5 weeks, Purkinje cells of Pvalb cKO animals were either SDH negative or were absent (Figure 3C), in coherence with the partial loss of Purkinje cells. We aimed at demonstrating that the SDH-negative neurons were frataxin deficient; however, due to the low levels of frataxin in DRG and cerebellum (i.e., ~30 ng FXN per mg of protein compared to ~150 ng FXN per mg of protein in the heart), we could not detect frataxin by immunohistochemistry with the available anti-frataxin antibodies. In non-neuronal FA mouse models, Fe-S cluster deficiency leads to IRP1 activation as a translational regulator leading to iron metabolism dysregulation.[19,26] In contrast with the clear iron accumulation observed in cardiomyocytes deficient for frataxin (MCK mutants; Figure S4F),[19] cerebellar Purkinje cells were negative for Perl's-enhanced iron staining at 13.5 weeks of age in *Pvalb* cKO (Figure S4G). However, upregulation of Transferrin receptor 1 (TfR1)

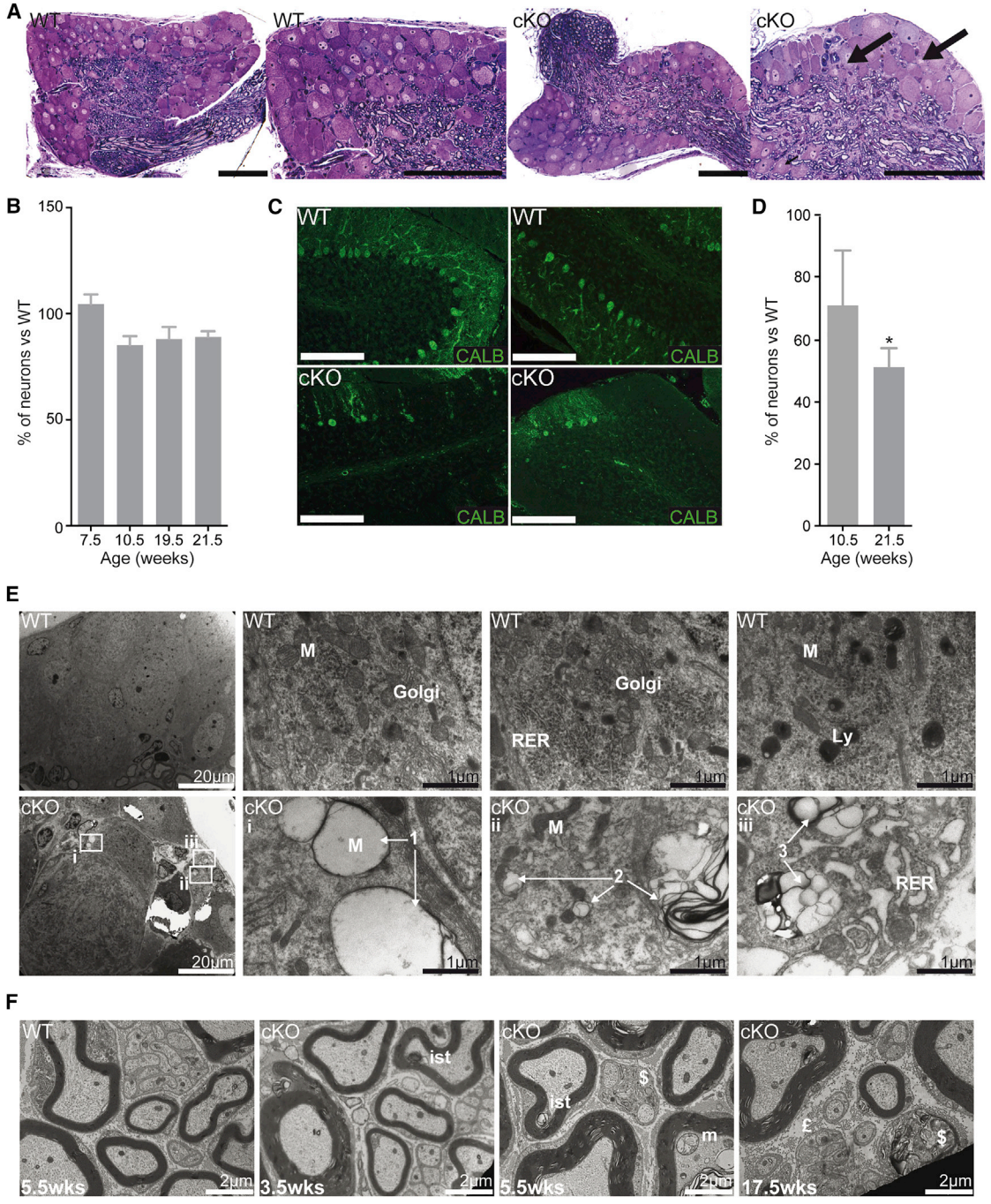

Figure 2. Neurodegeneration and Neuropathy in *Pvalb* cKO Mice

(A) Semithin sections of lumbar DRG at 7.5 weeks with arrows indicating vacuoles. n = 7,000 neurons scored. Scale bars, 100 µm. (B) Mean number of neurons per DRG normalized by DRG area in the lumbar section of the spinal cord. n = 3 or 4 mice and between 6,000 and 10,000 neurons scored per group and per age. (C) Calbindin staining on cerebellar section of control and *Pvalb* cKO mice at 21.5 weeks. Scale bars, 100 µm. (D) Purkinje cell loss in *Pvalb* cKO mice at 10.5 and 21.5 weeks assessed by scoring of Calbindin-positive cells. n = 4 mice and between 1,800 and 2,500 neurons scored per group and per age. (E) Ultrathin sections of lumbar DRG of WT and *Pvalb* cKO at 7.5 weeks with sign of cell death progression in large neurons with empty giant mitochondria (arrows 1), vacuoles (arrows 2) and with membrane invagination ending in a complete cell degeneration with dilated endoplasmic reticulum and larges vacuoles (arrows 3). M, mitochondria; Ly, lysosome; RER, rough endoplasmic reticulum. Scale bars, indicated sizes. (F) Ultrathin sections of sciatic nerves of WT and *Pvalb* cKO at 3.5, 5.5, and 17.5 weeks. ist, inner swelling tongue; £, fibrosis; m, abnormal mitochondria; $, degeneration. Scale bars, 2 µm. Data are represented as mean ± SEM. *$p < 0.05$.

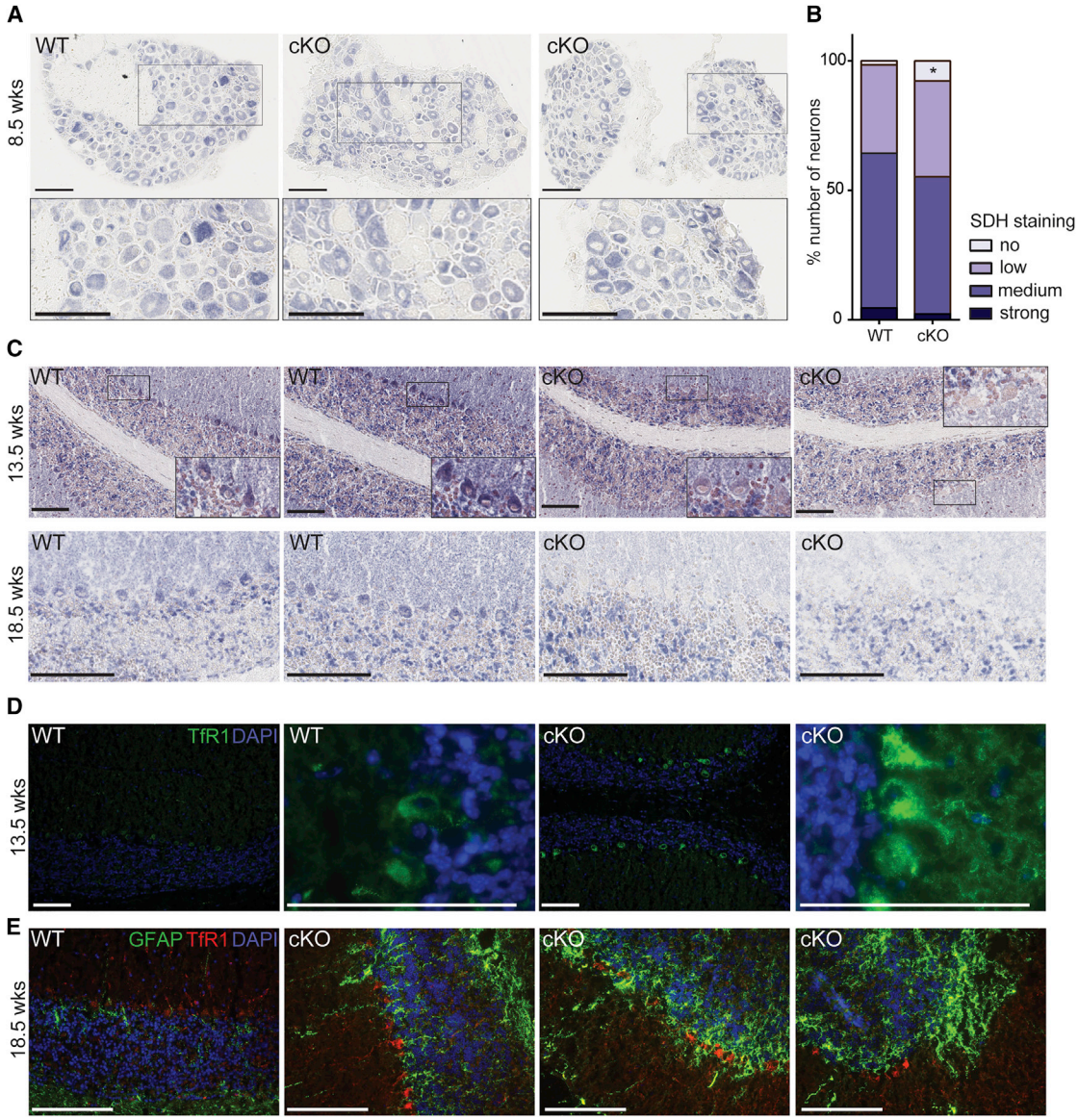

Figure 3. Fe-S Cluster Protein Deficit and Cellular Iron Metabolism Dysregulation in Some Neurons of *Pvalb* cKO Mice

(A) Representative SDH histoenzymatic activity staining in lumbar DRGs at 8.5 weeks of age WT and *Pvalb* cKO mice. Scale bars, 100 μm. (B) Scoring SDH staining intensity in lumbar DRG neurons at 5.5 weeks of age; n = 8,732 neurons counted from three WT animals and n = 11,019 neurons counted from four *Pvalb* cKO animals. *$p < 0.05$. (C) Representative SDH histoenzymatic activity staining in cerebellum at 13.5 and 18.5 weeks of age WT and *Pvalb* cKO mice with magnifications on Purkinje cells. Scale bars, 100 μm. (D) Representative images of TfR1 immunofluorescence (green) in cerebellum of WT and *Pvalb* cKO animals at 13.5 weeks of age. Scale bars, 100 μm. (E) Representative images of TfR1 (red) and GFAP (green) co-immunofluorescence in cerebellum of WT and *Pvalb* cKO animals at 18.5 weeks of age. Scale bars, 100 μm.

levels was detected in Purkinje cells in *Pvalb* cKO both at 13.5 and 18.5 weeks of age (Figures 3D and 3E), which could be a direct consequence of IRP1 activation in its iron response element (IRE) regulatory form.[26] Interestingly, the astrocyte marker GFAP signal was increased not only in the granular layer, but more particularly in the Purkinje cells and molecular layer in *Pvalb* cKO compare to controls (Figure 3E). The increase in GFAP is most likely a direct reflection of active astrogliosis coupled to Purkinje cell death.[27] All together, these results demonstrate that frataxin deficiency in neurons leads to an Fe-S cluster protein deficit and cellular iron dysregulation leading to cellular dysfunction and death.

Prevention of Progressive Loss of Sensory Defects after Treatment of Early-Symptomatic Pvalb cKO Mice

To investigate the potential of gene therapy for the treatment of the FA sensory ataxia and neuropathy, a single intravenous injection of AAV9-CAG-FXN-HA at a dose of 5×10^{13} vector genomes (vg)/kg was performed in 3.5-week-old early-symptomatic *Pvalb* cKO mice.

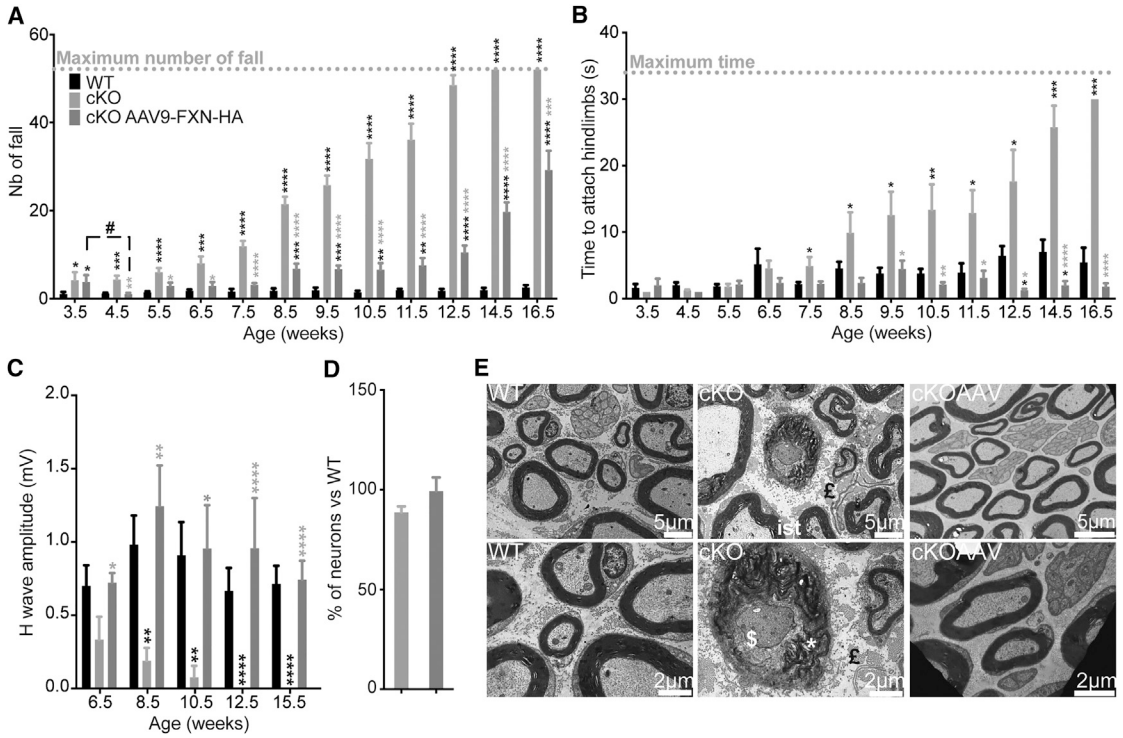

Figure 4. Evaluation of Early Symptomatic Treatment in *Pvalb* cKO Animals

(A) Notched-bar test analysis, number of footfalls is represented; n = 11 WT, n = 9 *Pvalb* cKO, and n = 9 *Pvalb* cKOAAV. (B) Hanging-wire test analysis, time needed to attach hindlimbs to the string is represented; n = 11 WT, n = 9 *Pvalb* cKO, and n = 9 *Pvalb* cKOAAV. (C) Amplitude of sensory wave (H-wave) was recorded after plantar sciatic nerve stimulation. n = 11 WT, n = 9 *Pvalb* cKO, and n = 9 *Pvalb* cKOAAV. (D) Mean number of neuron per DRG of WT and *Pvalb* (untreated and treated) was evaluated at the lumbar level of the spinal cord. n = 3 mice per group with n = 9,314 WT, n = 7,666 *Pvalb* cKO, and n = 7,610 *Pvalb* cKOAAV neurons scored. (E) Ultrathin sections of sciatic nerves of Pvalb treated at 17.5 weeks. ist, inner swelling tongue; £, fibrosis; *, myelin debris; $, degeneration. Scale bars, indicated sizes. Data are represented as mean ± SEM. *p < 0.05; **p < 0.01; ***p < 0.001; ****p < 0.0001. Black stars correspond to p value versus WT and gray stars versus untreated Pvalb cKO.

A significant coordination improvement in treated compared to untreated *Pvalb* cKO mice was observed in all tests performed (Figures 4A, 4B, and S5A). While, 1 week after treatment, a significant improvement of coordination on the notched-bar test was observed, the treated mice's performance progressively worsened starting at 8.5 weeks of age, although never to the level of untreated animals (Figure 4A). In contrast, treated *Pvalb* cKO mice remained undistinguishable from WT controls until euthanasia on the wire-hanging test (Figure 4B), showing a clear benefit on the peripheral sensory neuropathy. Consistent with the behavioral analysis, the defect in the sensorimotor reflex after sciatic nerve stimulation was completely prevented in treated *Pvalb* cKO mice (Figure 4C; Table S4).

Due to significant tremors, animals were sacrificed at 17.5 weeks of age. Biodistribution study of the AAV9-CAG-human frataxin (hFXN)-HA vector revealed a high transduction of the liver, a moderate transduction of the heart and brain, a milder transduction of the DRG, and a poor transduction of the spinal cord and cerebellum (Figure S5B). The transgenic human frataxin expression was 22 times the endogenous level in WT animals in the DRG (thoracic portion) (697 ng hFXN/mg protein) (Figure S5C). Western blot analysis showed that the majority of the transgenic human frataxin is matured and the absence of precursor accumulation (Figure S5D), as previously published.[12] Histologically, the trend in neuronal loss previously observed in *Pvalb* cKO in lumbar DRG was absent in the treated animal (Figure 4D). Furthermore, ultrastructural analysis of sciatic nerve showed no signs of degeneration, axonal loss, autophagy, or abnormal mitochondria in treated *Pvalb* cKO mice (Figure 4E), in agreement with the presence of normal somatosensory response.

AAV-hFXN Delivery Rapidly Rescues Sensory Ataxia in Late Symptomatic Pvalb Mice

While preventing the sensory ataxia is an important step, it is crucial to determine the therapeutic potential after the onset of the symptoms. Intravenous administration of AAV9-CAG-FXN-HA at a dose of 5×10^{13} vg/kg simultaneously with intracerebral deliveries of AAVrh.10-CAG-FXN-HA (1×10^{10} vg/deposit) in the striatum and the cerebellar white matter to target the CNS was performed post-symptomatically at 7.5 weeks of age. A complete correction of the peripheral fine coordination measured by the wire-hanging test was observed 1 week after treatment, which sustains overtime up to euthanasia (Figure 5A). On the notched-bar test, treated *Pvalb* cKO mice show a clear stabilization of the phenotype until 9.5 weeks of age then developed a progressive worsening of the phenotype

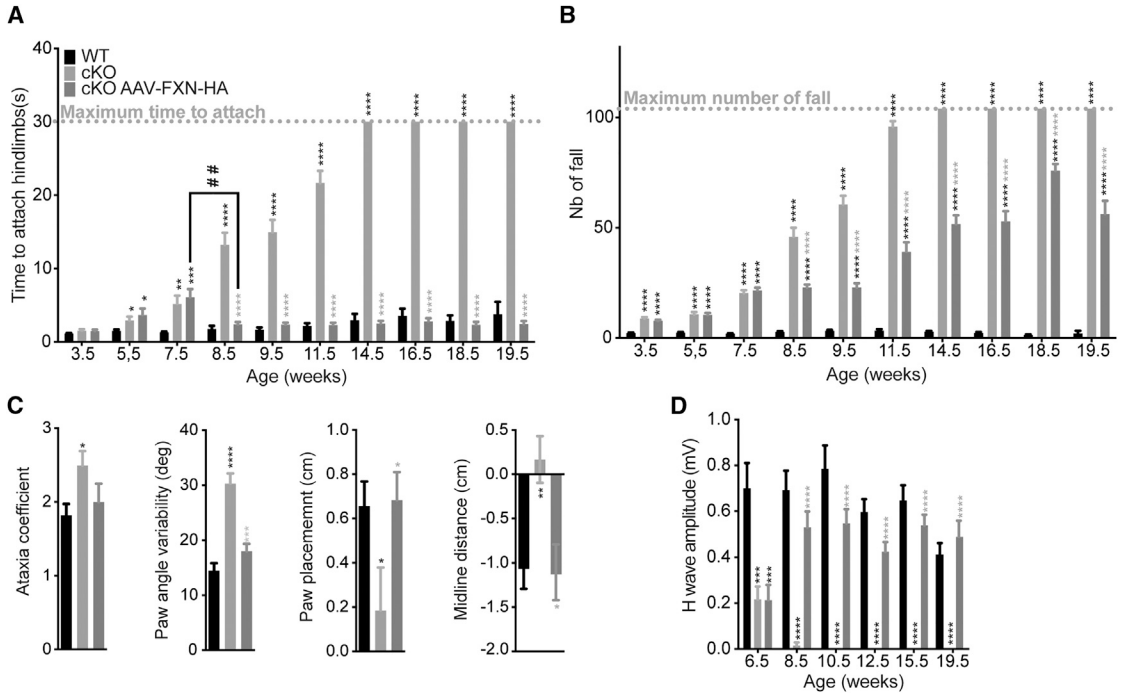

Figure 5. Rapid Correction of Neurological Phenotype after Post-symptomatic Treatment of *Pvalb* cKO Animals

(A) Hanging-wire test analysis, time needed to attach hindlimbs to the string is represented; n = 26 WT, n = 29 *Pvalb* cKO, and n = 32 *Pvalb* cKOAAV. (B) Notched-bar test analysis, number of footfalls is represented; n = 26 WT, n = 29 *Pvalb* cKO, and n = 32 *Pvalb* cKOAAV. (C) Ataxia coefficient, paw angle variability, paw placement, and midline distance measured after 2.5 s of walk on the DigitGait apparatus at 17.5 weeks of age; n = 8 WT, n = 6 *Pvalb* cKO, and n = 8 *Pvalb* cKOAAV. (D) Amplitude of sensory wave (H-wave) was recorded after plantar sciatic nerve stimulation; n = 26 WT, n = 29 *Pvalb* cKO, and n = 32 *Pvalb* cKOAAV. Data are represented as mean ± SEM. *p < 0.05; **p < 0.01; ***p < 0.001; ****p < 0.0001. Black stars correspond to p value versus WT and gray stars versus untreated Pvalb cKO.

(Figure 5B), as it was also observed on the rotarod (Figure S6A). Evaluation of the gait at 17.5 weeks of age by DigitGait analysis showed a complete correction of several parameters in the treated *Pvalb* cKO animals, including the ataxic coefficient, the paw angle variability, the paw placement, and the midline distance (Figure 5C). Concomitantly with the improvement of coordination and the ataxic phenotype, *Pvalb* cKO mice displayed a complete reversion of sensorimotor reflexes (Figure 5D; Table S5), with H-wave amplitudes within the normal range. Due to significant tremors, to avoid losing the animals of epileptic seizures and for ethical reasons, most animals were sacrificed at 18.5 weeks of age for histological and molecular analyses, with a few animals kept until 22.5 weeks for ultrastructural analysis.

Biodistribution study of the AAV-CAG-hFXN-HA vectors (both AAV9 and AAVrh10) reveals a high transduction of brain (cortex, cerebellum), a moderate transduction of brainstem in accordance with the intraparenchymal delivery of AAVrh.10, a milder transduction of the DRG, and quite poor transduction of the spinal cord (Figure S6B). Compared to what has been shown in pre-symptomatic treatment, DRG transduction is milder, in accordance with tropism and different transduction, depending on the age of delivery.[28] In agreement with the biodistribution of the vector, a widespread expression of hFXN-HA in the brain surrounding the injection site, especially in Purkinje cells and in striatum as well as in DRG neurons, was observed in the treated animals (Figures 6A–6D and S6C). Transgenic hFXN concentration was quantified by ELISA at 39.9 ng hFXN/mg protein in the DRG, corresponding to ~1.5 times the endogenous level, and at 176.3 ng hFXN/mg protein in the cerebellum, corresponding to 6 times the endogenous level (Figure S6D).

At 8.5 weeks of age, 1 week after treatment, the number of SDH-negative neurons in the DRG of treated *Pvalb* cKO animals did not differ from that of untreated animals (Figure 6E), despite the clear functional rescue at the physiological level. However, the trend in neuronal loss previously observed in lumbar DRG was absent in the treated animal, suggesting a protection against neuron loss at 18.5 weeks (Figure 6F). Moreover, ultrastructural analysis of the sciatic nerve of treated *Pvalb* mice at 22.5 weeks of age revealed a complete normal morphology with the absence of degeneration, axonal loss, autophagy, and abnormal mitochondria (Figure 6G), suggesting a complete regeneration of the sensory axonopathy. Interestingly, 1 week post-treatment, a clear process of regeneration (clearance of myelin debris, axon regrowth, and remyelination) was observed in treated animals (Figure S7A) with the nerve structure almost completely normal 2 weeks post-treatment (Figure S7B). All together, these results demonstrate a rapid and complete correction of the sensory neuropathy associated with frataxin deficiency by intravenous treatment using AAV9.

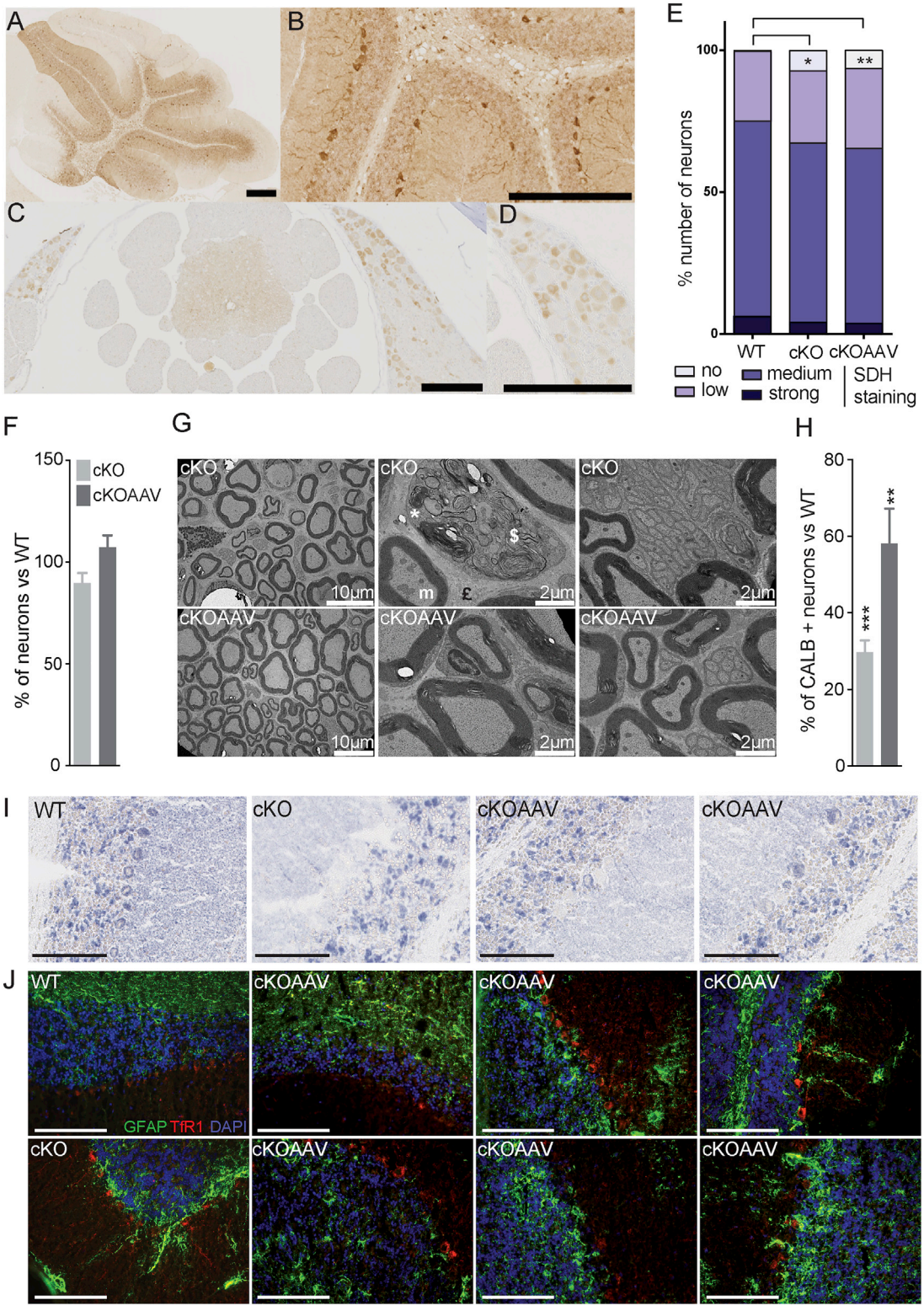

(legend on next page)

At 18.5 weeks, a significant prevention of Purkinje cell loss in the cerebellum occurred in treated animals (Figure 6H), although this was lobule dependent (Figure S6E), probably reflecting the non-homogeneous biodistribution of the vector (Figure S6C). A partial rescue of SDH-positive Purkinje cell was observed at 18.5 weeks in the treated animals (Figure 6I). Indeed, while in the cerebellum of untreated *Pvalb* cKO, few surviving Purkinje cells could be observed (all SDH negative); in treated animals, while the Purkinje cells appeared to be mostly preserved, the SDH staining varied from dark staining similar to the Purkinje cell of WT animals to SDH-negative staining, suggesting only a partial rescue. Similarly, the TfR1 and GFAP upregulation were partially corrected in treated animals, with some Purkinje cells presenting TfR1 and GFAP expression similar to WT Purkinje cells while other Purkinje cells (although less common) show various intermediate profiles of TfR1 and GFAP overexpression (Figure 6J). This is in agreement with the non-homogeneous biodistribution of the vector in the cerebellum.

DISCUSSION

Here, we report the generation of a new conditional mouse model for the ganglionopathy and sensory neuropathy associated with frataxin deficiency followed by the proof of concept of a gene therapy approach for the neuronal symptoms of FA. The new *Pvalb* cKO model developed a progressive loss of coordination and gait abnormalities, with a specific early onset of sensory defects followed by a cerebellar ataxia.

Through the characterization of this new model, several important findings were uncovered that might be of particular interest regarding the neuropathophysiology and cellular specificity in FA. One question that is still left unanswered in the field is the tissue specificity of the disease, and in particular why the large proprioceptive neurons are early and specifically affected compared to other neuronal populations, such as the nociceptive or mechanoreceptor neurons, for example. Quantitative measurements of frataxin by ELISA demonstrated not only more expression of frataxin in lumbar and thoracic DRGs than cervical DRGs, but more interestingly that proprioceptive neurons express 44%–66% of total frataxin protein of the DRGs, despite representing only 7.5% of total cell. Why would proprioceptive neurons express such high levels of frataxin compared to other cell types in the DRG is not known, but this may account partially for their higher vulnerability and premature loss in FA.[29] While it is technically impossible to measure sensorimotor reflexes in upper limbs due to the short length of the paw in mice, no signs of degeneration nor neuronal loss could be found in the radial or median nerve nor in thoracic and cervical DRG despite depletion of frataxin expression, suggesting that as in patients, the phenotype proceeds from lumbar to cervical region.[29] However, as the model exhibits premature death at 20 weeks due to epileptic seizures most likely as a consequence of frataxin depletion in cortical interneurons, it is not known whether degeneration of cervical DRG could occur with aging of the mice. Importantly, we showed that sensorimotor dysfunction by electrophysiology was an early event in the disease. While this is difficult to translate into human, the mouse model demonstrates that proprioceptive neurons completely deficient for frataxin can survive at least 7.5 weeks (as deletion occur around E17.5) and probably even more than 10 weeks of age, despite being dysfunctional early after frataxin deficiency. Considering that Schwann cells are not depleted for frataxin in the current model, our results demonstrate that proprioceptive neuronal dysfunction and pathology can occur in a cell-autonomous manner. However, it is likely that Schwann cells participate in the pathology in human, as low frataxin occurs in all tissues. Interestingly frataxin-deficient Purkinje cells in the cerebellum survive less time than frataxin-deficient proprioceptive neurons in DRG. While the reason for this difference is not known, the fact that the peripheral nervous system is regeneration competent might explain the better resistance of proprioceptive neurons to cell death. This resistance of proprioceptive neurons is a crucial point for therapeutical approaches for the sensory neuropathy, as most patients present a severe loss of proprioception at the time of the diagnosis, and the presence of proprioceptive neurons is not known. Finally, frataxin depletion in neurons, as in cardiac tissues, leads to an Fe-S cluster protein deficit, a secondary iron dysmetabolism, and mitochondrial defects before loss of cell. Whether iron accumulates in the nervous system is still under debate in the field, and recently iron accumulation was detected in cortical neurons of CRISPR-Cas9 frataxin-deficient mice.[30] In the present model, we did not detect any iron accumulation, probably because of the time course of the events. Indeed, iron accumulation in the CNS was shown to be a late event following frataxin deficiency.[30] Therefore, although the iron importer TfR1 is increased in the frataxin-deficient Purkinje cell, the neurons are lost most likely prior to sufficient iron accumulation to be detected by 3,3′-diaminobenzidine (DAB)-enhanced Perl's. In conclusion, the *Pvalb* cKO animals mimic several features of FA patients even if more severe on certain aspects and with a non-specific cerebral component due to full

Figure 6. Molecular and Histological Improvements after Post-symptomatic Treatment

(A–D) Representative images of FXN-HA expression in DRG and spinal cord (A and B) and cerebellum (C and D) of AAV-treated animals at 18.5 weeks. Scale bar, 100 μm. (E) Scoring of lumbar DRG neurons depending on the SDH staining intensity at 8.5 weeks of age; n = 6,574 neurons counted from two WT animals, n = 5,971 neurons counted from three *Pvalb* cKO animals, and n = 5,239 neurons counted from three *Pvalb* cKOAAV animals. (F) Mean number of neuron per DRG of WT and *Pvalb* cKO (untreated and treated) was evaluated at the lumbar level of the spinal cord; n = 6 mice with n = 13,375 WT, n = 11,581 *Pvalb* cKO, and n = 16,891 *Pvalb* cKOAAV neurons scored. (G) Ultrathin sections of sciatic nerves of 22.5-week *Pvalb* cKOAAV mice. £, fibrosis; m, abnormal mitochondria; *, myelin debris; $, degeneration. Scale bars, indicated sizes. (H) Mean number of Purkinje cell number in total in the cerebellum of WT and *Pvalb* cKO-treated and -untreated mice; n = 6 mice per group. (I) Representative SDH histoenzymatic staining of WT, untreated and treated *Pvalb* cKO animals in cerebellum at 18.5 weeks of age. Scale bars, 100 μm. (J) Representative images of TfR1 (red) and GFAP (green) co-immunofluorescence in cerebellum of WT, untreated, and treated *Pvalb* cKO animals at 18.5 weeks of age. Scale bars, 100 μm. Data are represented as mean ± SEM. *$p < 0.05$; **$p < 0.01$; ***$p < 0.001$. Black stars correspond to p value versus WT.

frataxin deficiency in cortical interneurons. In contrast to previously described models,[18] this new model has the advantage of having a specific proprioceptive phenotype from birth until 8 weeks of age and then develops a cerebellar ataxia with loss of frataxin in Purkinje cell and deep cerebellar nuclei.

Furthermore, our results demonstrate the capacity of intravenous AAV-hFXN delivery at a late symptomatic stage to rapidly and completely rescue the sensory neuropathy associated with frataxin deficiency. Importantly, our results suggest that dysfunctional frataxin-deficient proprioceptive neurons are in majority still alive for several weeks despite their severely affected nerve structure, and their phenotype can be completely reversed, demonstrating high plasticity. Furthermore, the rapidity of the rescue (1 week after treatment) demonstrates that little frataxin is needed to permit the neurons to regenerate and fully recover their nerve structure. This is in contrast to the recently published results from the doxycycling-inducible systemic knockdown of frataxin, which show only partial correction of the ganglionopathy and a mild improvement of axonal neuropathy after 8 weeks of frataxin rescue.[31] In addition, through intraparenchymal AAVrh10-hFXN delivery, we demonstrate a partial rescue and prevention of Purkinje cell loss. The partial rescue is mainly due to the limited diffusion of the virus and the consecutive transduction of Purkinje cells, which correlates with the correction of SDH activity as well as TfR1 and GFAP dysregulation. The absence of full transduction of the Purkinje cells as well the cortical interneurons is most likely responsible for the tremors and epileptic attacks in the treated *Pvalb* cKO.

In conclusion, our results demonstrate the strong potential of AAV delivery to restore frataxin expression in DRG and rescue the ganglionopathy and sensory neuropathy associated to frataxin deficiency, even in severely affected animals. While this is encouraging for the development of a therapeutic approach in clinical settings, the FA neuropathology in humans is complex, and the status of proprioceptive neurons in FA patients in the early stages of the disease remains to be determined. Mice still developed a cerebral phenotype; however, this is not a phenotype occurring in FA patients, although it is important to target the Purkinje cell and the dentate nucleus in the cerebellum of FA patients. To improve the therapeutical approach, it would be of interest to optimize overall brain transduction, especially the cerebellum, with new generation of AAV vectors with an optimized capsid, such as the newly described PHPeB vectors.[32]

MATERIALS AND METHODS

Animals

Mice carrying the conditional allele for the frataxin gene ($Fxn^{L3/L3}$) as described previously[19] were mated with B6;129P2-$Pvalb^{tm1(Cre)Arbr/J}$ (https://www.jax.org/strain/008069; Jackson Laboratory, Maine, USA)[21] in order to generate $Fxn^{L3/L-}$; $Pvalb^{tm1(Cre)Arbr/J}$ (named *Pvalb* cKO thereafter) and the $Fxn^{+/L3}$ mice used as controls. To monitor tissue specificity and temporal expression of Cre recombinase activity, B6;129P2-$Pvalb^{tm1(Cre)Arbr/J}$ mice were mated with a reporter B6;129S4-$Gt(ROSA)26Sor^{tm1Sor}$/J (https://www.jax.org/strain/003309).[33] Animals were maintained in a temperature- and humidity-controlled animal facility with a 12-hr light-dark cycle and free access to water and a standard rodent chow (D03, SAFE, Villemoisson-sur-Orge, France) and supplement after 7.5 weeks of age with jellified food (gel diet A03 SAFE or Dietgel 76A clear H20). All animal procedures were approved by the local ethical committee (C2EA-17, agreements 604 and 2852) and were performed in accordance with the Guide for the Care and the Use of Laboratory Animals (US NIH).

For early symptomatic studies, 3.5-week-old mice were anesthetized by intraperitoneal (i.p.) injection with ketamine and xylazine (130/13 mg/kg) to allow retro-orbital intravenous administration of AAV9-CAG-FXN-HA at a dose of 5×10^{13} vg/kg. Untreated *Pvalb* cKO and WT mice were injected with equivalent volumes of saline solution. For late symptomatic studies, 7.5-week-old mice were anesthetized by i.p. injection with ketamine and xylazine (130/13 mg/kg), positioned on the stereotactic frame (David Kopf Instruments, Tujunga, USA) and injected bilaterally in the striatum and in the white matter of the cerebellum with an AAVrh.10-CAG-FXN-HA at a dose of 1×10^{10} vg/deposit (Table S6). Injections were done using a 30G blunt needle attached to a 10 μL Hamilton syringe (Hamilton, USA) at a rate of 0.2 μL/min. Animals were then intravenously injected with AAV9-CAG-FXN-HA at a dose of 5×10^{13} vg/kg. To avoid suffering, animals received an injection of buprecare (0.3 mg/kg) before waking up (Animal Care, France). Untreated *Pvalb* cKO and WT mice were injected with equivalent volumes of saline solution. Animals were monitored daily after the surgery. The combination of AAV serotypes used was based on published[34] and preliminary tests. Pre-symptomatic AAVrh.10-CAG-FXN-HA IV delivery at a dose of 5×10^{13} vg/kg, did not prevent the onset sensory ataxia in Pvalb cKO animals measured by electromyogram (EMG) (data not shown). Furthermore, comparison of intraparenchymal delivery of AAVrh10-GFP and AAV9-GFP demonstrated better neuronal transduction efficiency for AAVrh10 (data not shown).

The AAV vectors were the same as the ones used in the previous gene therapy study[12] with final titers of 8.5×10^{13} vg/mL for the AAV9-CAG-hFXN-HA and 5.5×10^{13} vg/mL for the AAVrh.10-CAG-hFXN-HA.

Behavioral Analysis

Behavioral experiments were conducted to evaluate motor and muscular function. Coordination was evaluated using the notched-bar test (scored number of falls of the upper or lower limbs) and the wire-hanging test (scored the time needed by animal to attach their hindlimbs) as previously described[35] but without training. General motor capacities were tested using the accelerating rotarod LE8200 (Bioseb, France), and open field activity was measured on the photocell actimeter LE8811 (Bioseb, France), as previously described (https://www.mousephenotype.org/). Animals were scored weekly for each test from 3.5 weeks of age until euthanasia, in the following order: wire-hanging test, notched-bar test, rotarod, and open field. Gait analysis was performed at 13.5 weeks or at 18.5 weeks of age using a DigitGait Apparatus (Mouse Specific, Boston, USA), as described previously.[36] The paws of the mice were captured by video

during treadmill locomotion at a speed of 21 cm/s for at least 5 s of proper gait, and analysis was performed using the DigitGait Analyzer software (Mouse Specific, Boston, USA).

Electromyogram analyses were performed using the Natus UltraProS100 apparatus (Mag2Health, France). Mice were anesthetized using i.p. injection with ketamine/xylazine (130/13 mg/kg). Animals were maintained at 37°C during the whole experiment until wakeup. Latency and amplitude of M and H-waves were recorded in the plantar hindpaw muscle after sciatic nerve stimulation (0.1 ms and 8 mA intensity). An additional recording of the M-wave was performed in the gastrocnemius muscle. Measurements were performed every 2 weeks starting at 3.5 weeks of age.

Histology

For histological analyses, mice were killed by i.p. injection of ketamine-xylazine (300/13 mg/kg) and perfused with 10 mL of PBS. Various tissues were dissected and either fixed in paraformaldehyde (PFA) and embedded in paraffin or directly embedded in Shandon Cryomatrix embedding resin (Thermo Fisher Scientific) and snap-frozen in isopentane chilled on dry ice. For spinal cord and DRG analysis, prior to the paraffin embedding, the column was decalcified in EDTA 0.34 M (pH 7.4) for 14 days, and the spinal cord was divided into cervical, thoracic, and lumbar levels. DRG neurons were scored on paraffin sections (5 μm) stained with H&E. The number of neurons was normalized by the area of the DRG section. DAB-enhanced Perl's iron staining was performed on 8-μm tissue cryosections as previously described.[12] β-galactosidase staining was performed on 10-μm cryopreserved sections with a protocol adapted from Sanes et al.[37]

HA immunodetection was performed on paraffin sections using Vectastain ABC kit followed by DAB enhancement according to manufacturer's protocol (Vector Labs), with slight modification, including epitope unmasking in 10 mM Tris, 1 mM EDTA, 0.1% Tween 20 (pH 8.75) for 45 min at 95°C, and images acquired on a Hamamatsu NanoZoomer 2.0 slide scanner. Succinate dehydrogenase (SDH) activity was determined on 8-μm cryosections of tissues, as previously described[19] with adapted incubation time with the substrate solution (25 min for the DRG sections, 30 min for the brain sections). Images were acquired using the Hamamatsu NanoZoomer 2.0 slide scanner. DRG neurons were then scored on the intensity of the SDH signal: strong, medium, low, and no SDH staining. All experiments were performed blindly.

Calbindin, MBP, and Neurofilament 200-kDa (NF-200) immunofluorescences were performed on paraffin sections according to previous protocols.[38,39]

TfR1 and GFAP immunofluorescence single labeling or co-labeling were performed on 8-μm 4% PFA fixed cryosections. Sections were mounted using ProLong Gold antifade reagent (Invitrogen), and images were recorded with a Leica DM4000B-M microscope equipped with a Coolsnap HQ2 camera and Micromanager software (see Table S7 for antibodies dilutions and references).

For electron microscopy analysis, animals were perfused with 5 mL of PBS and 10 mL 4% PFA in saline, and tissues were fixed in 2.5% PFA/2.5% glutaraldehyde in cacodylate buffer, and samples were processed as previously described.[12,19]

Molecular Biology

Mice were killed by i.p. injection of ketamine-xylazine (300 mg/kg; 30 mg/kg), and samples for biochemical and molecular analyses were immediately frozen in liquid nitrogen. Protein extractions and western blot were performed as previously described.[12] Twelve micrograms of proteins were loaded on the gels, and the membranes were incubated with the different antibodies (Table S7) detected with SuperSignal West Pico chemiluminescent substrate (Thermo Fisher Scientific) or SuperSignal West Femto maximum sensitivity substrate (for frataxin detection). Chemiluminescent images were acquired on the Amersham Imager 600 (GE Healthcare Life Sciences). The activity of the respiratory chain enzyme SDH (complex II) was determined as previously described.[19,40] Mouse and human frataxin were quantified in DRG (cervical, thoracic, and lumbar) and cerebellum extracts using the mouse frataxin ELISA and human frataxin ELISA kits (Abcam, ab199078, and Abcam, ab176112, respectively) according to the manufacturer's protocol.

Vector Genome Copy Number was measured by qPCR on extracted genomic DNA from DRG, spinal cord (cervical, thoracic, and lumbar levels), brain, cerebellum, heart, and liver using the Light Cycler 480 SYBR Green I Master (Roche, France). The results (vector genome copy number per cell) were expressed as n-fold differences in the transgene sequence copy number relative to the *Adck3* gene copy as internal standard (number of viral genome copy for 2N genome).

Statistical Analyses

All data are presented as mean ± SEM. Statistical analysis was carried out using GraphPad Prism software (La Jolla, USA). Student's t tests were used to compare group, and a value of $p < 0.05$ was considered as significant.

SUPPLEMENTAL INFORMATION

Supplemental Information includes Supplemental Results, seven figures, and seven tables and can be found with this article online at https://doi.org/10.1016/j.ymthe.2018.05.006.

AUTHOR CONTRIBUTIONS

Conceptualization, F.P., C.d.M., H.P.; Methodology, F.P., C.d.M., H.P.; Investigation, F.P., C.d.M., N.V., A.E.; Resources, L.R.; Writing – Original Draft, F.P., C.d.M., H.P.; Writing – Review & Editing, F.P., C.d.M., H.P.; Funding Acquisition, H.P.; Supervision, H.P.; F.P. and C.d.M. contributed equally to the study.

CONFLICTS OF INTEREST

H.P. is scientific consultant to Voyager Therapeutics. All other authors declare no competing financial interests.

ACKNOWLEDGMENTS

We thank Nadia Messaddeq from the IGBMC imaging platform for EM analysis and Véronique Blouin (Institut de Recherche Thérapeutique, INSERM UMR 1089) for vector production. This work was supported by the US Friedreich Ataxia Research Alliance (to H.P.) and a personal donation from the Lurton family (to H.P.). C.d.M. is a recipient of a 4th year PhD fellowship from the Association Française pour l'Ataxie de Friedreich. This study was supported by the grant ANR-10-LABX-0030-INRT, a French State fund managed by the Agence Nationale de la Recherche under the frame program Investissement d'Avenir ANR-10-IDEX-0002-02.

REFERENCES

1. Harding, A.E. (1981). Friedreich's ataxia: a clinical and genetic study of 90 families with an analysis of early diagnostic criteria and intrafamilial clustering of clinical features. Brain *104*, 589–620.
2. Pandolfo, M. (2009). Friedreich ataxia: the clinical picture. J. Neurol. *256* (*Suppl 1*), 3–8.
3. Koeppen, A.H., and Mazurkiewicz, J.E. (2013). Friedreich ataxia: neuropathology revised. J. Neuropathol. Exp. Neurol. *72*, 78–90.
4. Koeppen, A.H., Ramirez, R.L., Becker, A.B., and Mazurkiewicz, J.E. (2016). Dorsal root ganglia in Friedreich ataxia: satellite cell proliferation and inflammation. Acta Neuropathol. Commun. *4*, 46.
5. Kemp, K.C., Cook, A.J., Redondo, J., Kurian, K.M., Scolding, N.J., and Wilkins, A. (2016). Purkinje cell injury, structural plasticity and fusion in patients with Friedreich's ataxia. Acta Neuropathol. Commun. *4*, 53.
6. Selvadurai, L.P., Harding, I.H., Corben, L.A., and Georgiou-Karistianis, N. (2018). Cerebral abnormalities in Friedreich ataxia: A review. Neurosci. Biobehav. Rev. *84*, 394–406.
7. Tsou, A.Y., Paulsen, E.K., Lagedrost, S.J., Perlman, S.L., Mathews, K.D., Wilmot, G.R., Ravina, B., Koeppen, A.H., and Lynch, D.R. (2011). Mortality in Friedreich ataxia. J. Neurol. Sci. *307*, 46–49.
8. Campuzano, V., Montermini, L., Molto, M.D., Pianese, L., Cossee, M., Cavalcanti, F., Monros, E., Rodius, F., Duclos, F., Monticelli, A., et al. (1996). Friedreich's ataxia: autosomal recessive disease caused by an intronic GAA triplet repeat expansion. Science *271*, 1423–1427.
9. Kumari, D., and Usdin, K. (2012). Is Friedreich ataxia an epigenetic disorder? Clin. Epigenetics *4*, 2.
10. Schmucker, S., Martelli, A., Colin, F., Page, A., Wattenhofer-Donzé, M., Reutenauer, L., and Puccio, H. (2011). Mammalian frataxin: an essential function for cellular viability through an interaction with a preformed ISCU/NFS1/ISD11 iron-sulfur assembly complex. PLoS ONE *6*, e16199.
11. Colin, F., Martelli, A., Clémancey, M., Latour, J.M., Gambarelli, S., Zeppieri, L., Birck, C., Page, A., Puccio, H., and Ollagnier de Choudens, S. (2013). Mammalian frataxin controls sulfur production and iron entry during de novo Fe4S4 cluster assembly. J. Am. Chem. Soc. *135*, 733–740.
12. Perdomini, M., Belbellaa, B., Monassier, L., Reutenauer, L., Messaddeq, N., Cartier, N., Crystal, R.G., Aubourg, P., and Puccio, H. (2014). Prevention and reversal of severe mitochondrial cardiomyopathy by gene therapy in a mouse model of Friedreich's ataxia. Nat. Med. *20*, 542–547.
13. Miranda, C.J., Santos, M.M., Ohshima, K., Smith, J., Li, L., Bunting, M., Cossée, M., Koenig, M., Sequeiros, J., Kaplan, J., and Pandolfo, M. (2002). Frataxin knockin mouse. FEBS Lett. *512*, 291–297.
14. Pook, M.A., Al-Mahdawi, S., Carroll, C.J., Cossée, M., Puccio, H., Lawrence, L., Clark, P., Lowrie, M.B., Bradley, J.L., Cooper, J.M., et al. (2001). Rescue of the Friedreich's ataxia knockout mouse by human YAC transgenesis. Neurogenetics *3*, 185–193.
15. Al-Mahdawi, S., Pinto, R.M., Ruddle, P., Carroll, C., Webster, Z., and Pook, M. (2004). GAA repeat instability in Friedreich ataxia YAC transgenic mice. Genomics *84*, 301–310.
16. Al-Mahdawi, S., Pinto, R.M., Varshney, D., Lawrence, L., Lowrie, M.B., Hughes, S., Webster, Z., Blake, J., Cooper, J.M., King, R., and Pook, M.A. (2006). GAA repeat expansion mutation mouse models of Friedreich ataxia exhibit oxidative stress leading to progressive neuronal and cardiac pathology. Genomics *88*, 580–590.
17. Anjomani Virmouni, S., Ezzatizadeh, V., Sandi, C., Sandi, M., Al-Mahdawi, S., Chutake, Y., and Pook, M.A. (2015). A novel GAA-repeat-expansion-based mouse model of Friedreich's ataxia. Dis. Model. Mech. *8*, 225–235.
18. Perdomini, M., Hick, A., Puccio, H., and Pook, M.A. (2013). Animal and cellular models of Friedreich ataxia. J. Neurochem. *126* (*Suppl 1*), 65–79.
19. Puccio, H., Simon, D., Cossée, M., Criqui-Filipe, P., Tiziano, F., Melki, J., Hindelang, C., Matyas, R., Rustin, P., and Koenig, M. (2001). Mouse models for Friedreich ataxia exhibit cardiomyopathy, sensory nerve defect and Fe-S enzyme deficiency followed by intramitochondrial iron deposits. Nat. Genet. *27*, 181–186.
20. Simon, D., Seznec, H., Gansmuller, A., Carelle, N., Weber, P., Metzger, D., Rustin, P., Koenig, M., and Puccio, H. (2004). Friedreich ataxia mouse models with progressive cerebellar and sensory ataxia reveal autophagic neurodegeneration in dorsal root ganglia. J. Neurosci. *24*, 1987–1995.
21. Hippenmeyer, S., Vrieseling, E., Sigrist, M., Portmann, T., Laengle, C., Ladle, D.R., and Arber, S. (2005). A developmental switch in the response of DRG neurons to ETS transcription factor signaling. PLoS Biol. *3*, e159.
22. Marmigère, F., and Ernfors, P. (2007). Specification and connectivity of neuronal subtypes in the sensory lineage. Nat. Rev. Neurosci. *8*, 114–127.
23. Zacharová, G., and Paleček, J. (2009). Parvalbumin and TRPV1 receptor expression in dorsal root ganglion neurons after acute peripheral inflammation. Physiol. Res. *58*, 305–309.
24. Rötig, A., de Lonlay, P., Chretien, D., Foury, F., Koenig, M., Sidi, D., Munnich, A., and Rustin, P. (1997). Aconitase and mitochondrial iron-sulphur protein deficiency in Friedreich ataxia. Nat. Genet. *17*, 215–217.
25. Lange, W. (1975). Cell number and cell density in the cerebellar cortex of man and some other mammals. Cell Tissue Res. *157*, 115–124.
26. Martelli, A., Schmucker, S., Reutenauer, L., Mathieu, J.R.R., Peyssonnaux, C., Karim, Z., Puy, H., Galy, B., Hentze, M.W., and Puccio, H. (2015). Iron regulatory protein 1 sustains mitochondrial iron loading and function in frataxin deficiency. Cell Metab. *21*, 311–323.
27. Eng, L.F., and Ghirnikar, R.S. (1994). GFAP and astrogliosis. Brain Pathol. *4*, 229–237.
28. Bostick, B., Ghosh, A., Yue, Y., Long, C., and Duan, D. (2007). Systemic AAV-9 transduction in mice is influenced by animal age but not by the route of administration. Gene Ther. *14*, 1605–1609.
29. Koeppen, A.H., Morral, J.A., Davis, A.N., Qian, J., Petrocine, S.V., Knutson, M.D., Gibson, W.M., Cusack, M.J., and Li, D. (2009). The dorsal root ganglion in Friedreich's ataxia. Acta Neuropathol. *118*, 763–776.
30. Chen, K., Ho, T.S.Y., Lin, G., Tan, K.L., Rasband, M.N., and Bellen, H.J. (2016). Loss of Frataxin activates the iron/sphingolipid/PDK1/Mef2 pathway in mammals. eLife *5*, 1–14.
31. Chandran, V., Gao, K., Swarup, V., Versano, R., Dong, H., Jordan, M.C., and Geschwind, D.H. (2017). Inducible and reversible phenotypes in a novel mouse model of Friedreich's Ataxia. eLife *6*, 1–41.
32. Chan, K.Y., Jang, M.J., Yoo, B.B., Greenbaum, A., Ravi, N., Wu, W.L., Sánchez-Guardado, L., Lois, C., Mazmanian, S.K., Deverman, B.E., and Gradinaru, V. (2017). Engineered AAVs for efficient noninvasive gene delivery to the central and peripheral nervous systems. Nat. Neurosci. *20*, 1172–1179.
33. Soriano, P. (1999). Generalized lacZ expression with the ROSA26 Cre reporter strain. Nat. Genet. *21*, 70–71.
34. Piguet, F., Sondhi, D., Piraud, M., Fouquet, F., Hackett, N.R., Ahouansou, O., Vanier, M.T., Bieche, I., Aubourg, P., Crystal, R.G., et al. (2012). Correction of brain oligodendrocytes by AAVrh.10 intracerebral gene therapy in metachromatic leukodystrophy mice. Hum. Gene Ther. *23*, 903–914.
35. Arbogast, T., Raveau, M., Chevalier, C., Nalesso, V., Dembele, D., Jacobs, H., Wendling, O., Roux, M., Duchon, A., and Herault, Y. (2015). Deletion of the App-Runx1 region in mice models human partial monosomy 21. Dis. Model. Mech. *8*, 623–634.

36. Wooley, C.M., Sher, R.B., Kale, A., Frankel, W.N., Cox, G.A., and Seburn, K.L. (2005). Gait analysis detects early changes in transgenic SOD1(G93A) mice. Muscle Nerve *32*, 43–50.

37. Sanes, J.R., Rubenstein, J.L., and Nicolas, J.F. (1986). Use of a recombinant retrovirus to study post-implantation cell lineage in mouse embryos. EMBO J. *5*, 3133–3142.

38. Sevin, C., Benraiss, A., Van Dam, D., Bonnin, D., Nagels, G., Verot, L., Laurendeau, I., Vidaud, M., Gieselmann, V., Vanier, M., et al. (2006). Intracerebral adeno-associated virus-mediated gene transfer in rapidly progressive forms of metachromatic leukodystrophy. Hum. Mol. Genet. *15*, 53–64.

39. Bolino, A., Piguet, F., Alberizzi, V., Pellegatta, M., Rivellini, C., Guerrero-Valero, M., Noseda, R., Brombin, C., Nonis, A., D'Adamo, P., et al. (2016). Niacin-mediated Tace activation ameliorates CMT neuropathies with focal hypermyelination. EMBO Mol. Med. *8*, 1438–1454.

40. Martelli, A., Friedman, L.S., Reutenauer, L., Messaddeq, N., Perlman, S.L., Lynch, D.R., Fedosov, K., Schulz, J.B., Pandolfo, M., and Puccio, H. (2012). Clinical data and characterization of the liver conditional mouse model exclude neoplasia as a non-neurological manifestation associated with Friedreich's ataxia. Dis. Model. Mech. *5*, 860–869.

YMTHE, Volume *26*

Supplemental Information

Rapid and Complete Reversal of Sensory Ataxia by Gene Therapy in a Novel Model of Friedreich Ataxia

Françoise Piguet, Charline de Montigny, Nadège Vaucamps, Laurence Reutenauer, Aurélie Eisenmann, and Hélène Puccio

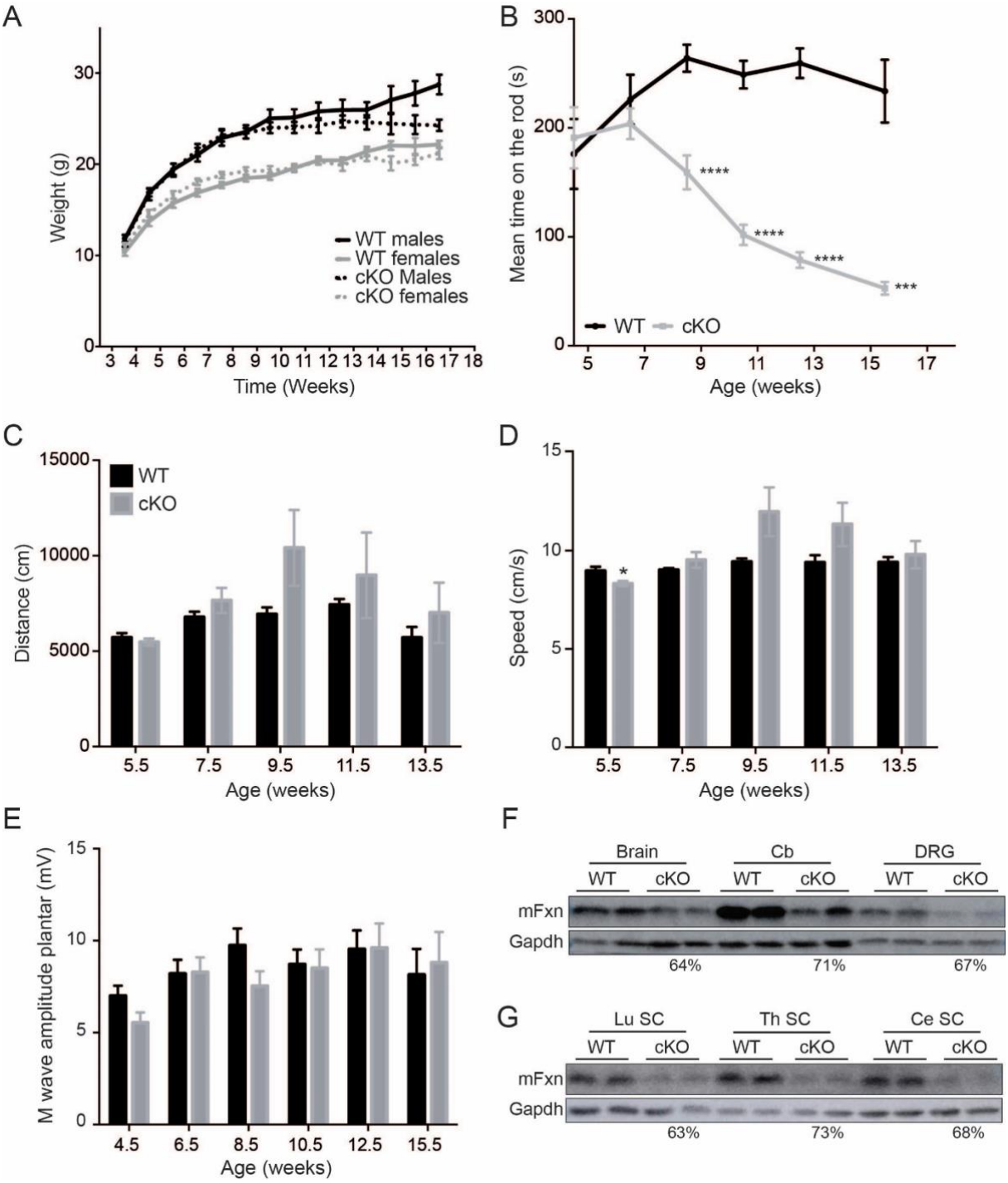

Figure S1: *Pvalb* cKO mice characterization

(**A**) Growth curve, N= 10 WT and N= 11 *Pvalb* cKO. (**B**) Evaluation of rotarod performances, N= 10 WT and N= 11 *Pvalb* cKO. (**C**-**D**) Openfield analysis with measurement of the distance (**C**) and mean speed in the arena (**D**) in a 20 min activity session, N= 6 WT and N= 7 *Pvalb* cKO**.** (**E**) Amplitude of motor wave (M-Wave) were recorded after plantar sciatic nerve stimulation, N= 6 WT and N= 7 *Pvalb* cKO. *Pvalb* cKO animals did not differ from control animals. (**F**-**G**) Expression of mouse Frataxin (mFXN) protein in brain, cerebellum, total DRG (**F**) lumbar, thoracic and cervical spinal cord (LuSC, Th SC, Ce SC, respectively) (**G**) from WT and *Pvalb* cKO mice at 7.5 weeks of age. Percentage of depletion in each tissue is indicated under the western blot. Data are represented as mean +/- SEM. *p<0.05; **p<0.01; ***p<0.001; ****p<0.0001.

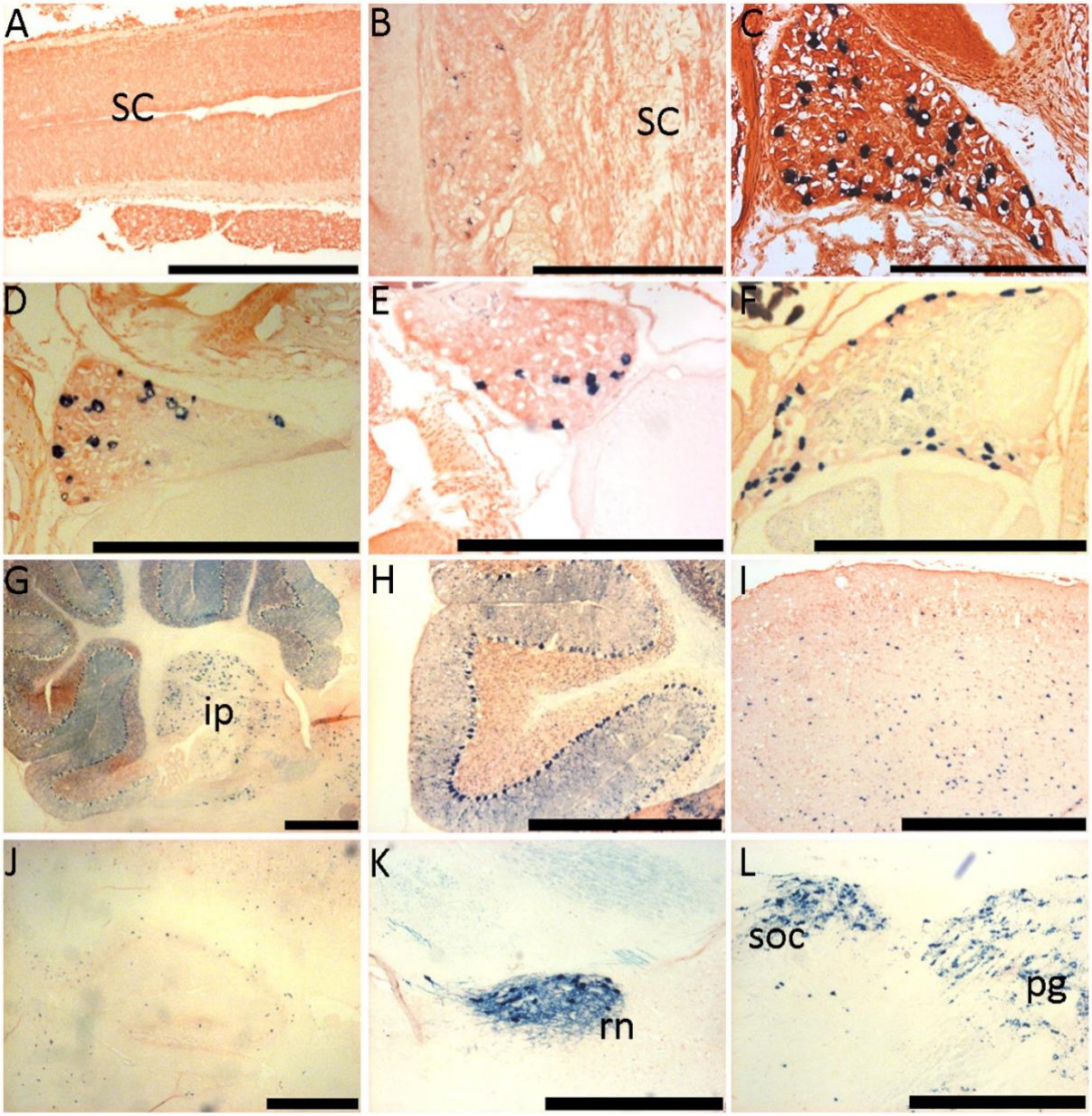

Figure S2: *Pvalb*-Cre expression in DRG and brain overtime.
LacZ staining on frozen section of DRG at E14.5 (**A**), E17.5 (**B**) and p8 (**C**) and at 21.5 weeks in cervical (**D**), thoracic (**E**) and lumbar (**F**) DRG. Enlargements of cerebellum (**G-H**), cortex (**I**), hippocampus (**J**), midbrain (**K**) and pons (**L**) at 21.5 weeks; ip: interposed nucleus, rn: red nucleus, soc: superior olive complex, pg: pontine grey. Scale bars, 500µm**.**

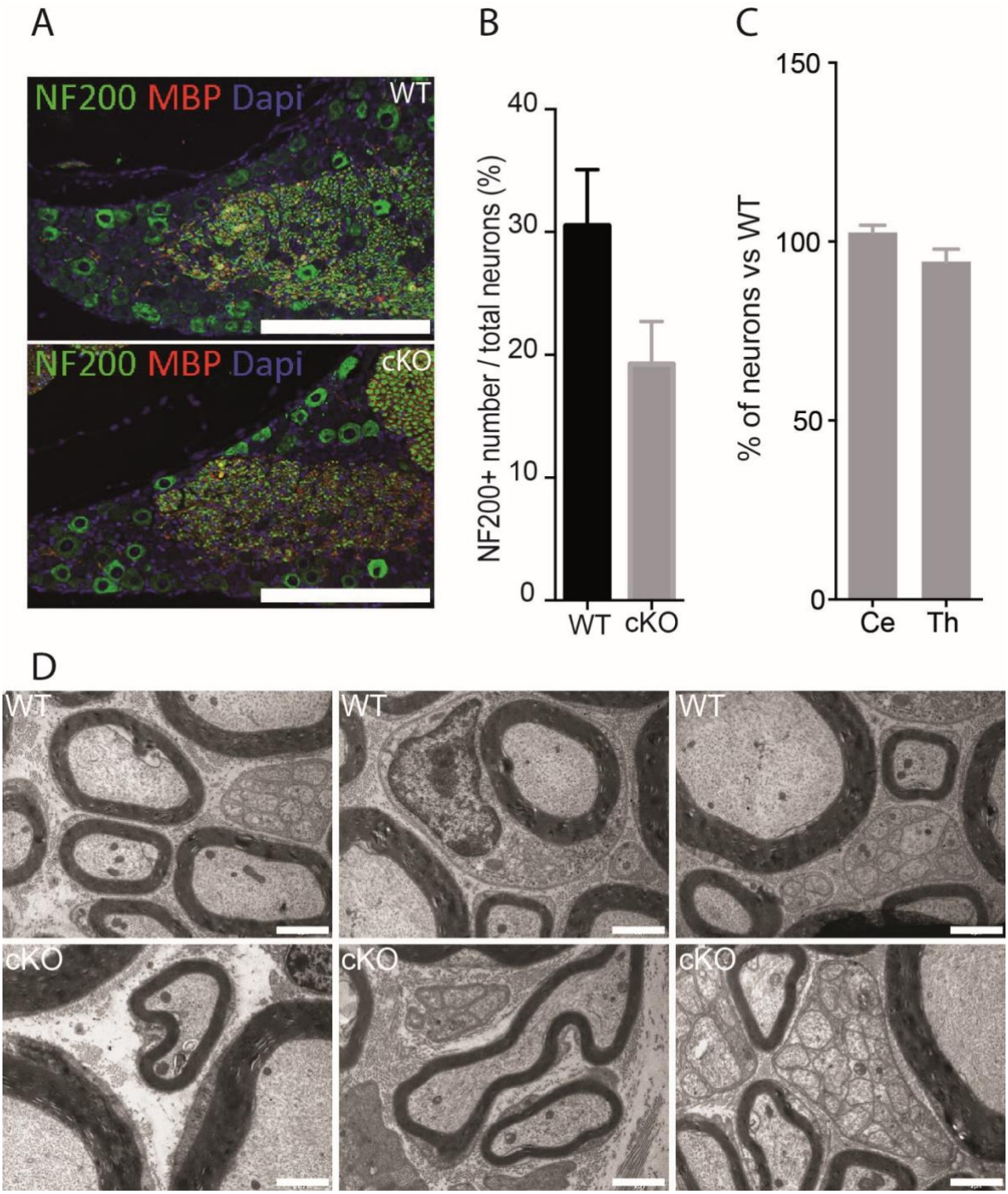

Figure S3: Histological evaluation of *Pvalb* cKO animals.
(**A**) Representative images of NF200 and MBP co-staining in 21.5 weeks DRG. Scale bars, 200µm. (**B**) Scoring of neurons co-stained with NF200 and MBP showed a 30% loss of large neurons within DRG, N= 4 WT and N= 4 *Pvalb* cKO scored. (**C**) Mean number of neuron per DRG of WT and *Pvalb* cKO was evaluated at the cervical and thoracic level of the spinal cord, N= 3-4 mice analyzed per group for the cervical and thoracic portions. (**D**) Ultrathin sections of radial and median nerves at 18.5 weeks. Scale bars, 2µm. Data are represented as mean +/- SEM.

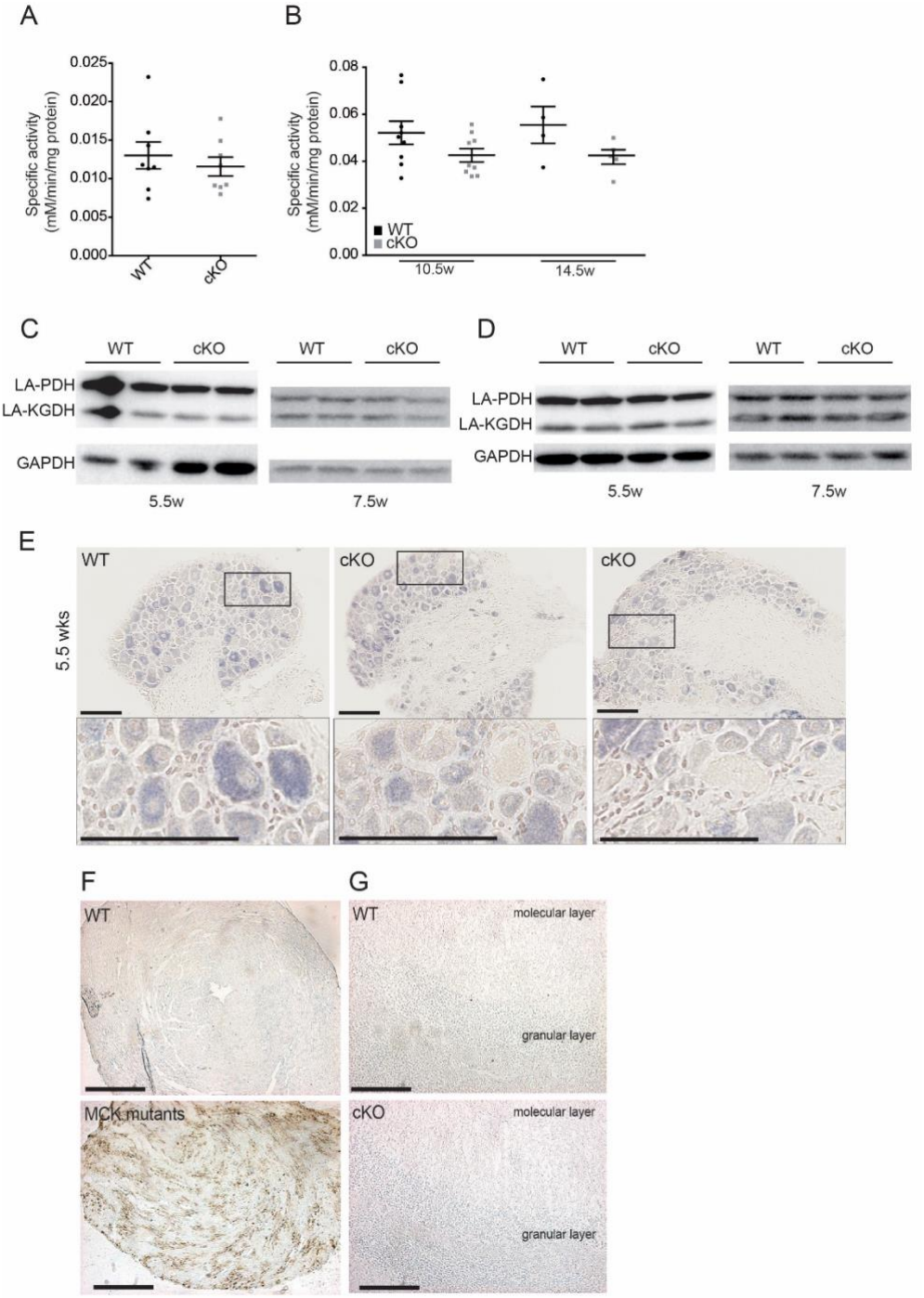

Figure S4: Fe-S cluster protein deficit is not detected on total protein extracted samples.
(**A**) SDH specific enzymatic activity on lumbar DRG at 7.5 weeks of age, N = 8 per group. (**B**) SDH specific enzymatic activity on cerebellum samples at 10.5 and 14.5 weeks of age, N= 9 per group at 10.5 weeks, N= 4 per group at 14.5 weeks. (**C-D**) Expression of Fe-S cluster apoprotein in DRG (**C**) and cerebellum (**D**) samples from WT and *Pvalb* cKO mice at 5.5 and 7.5 weeks of age. LA-PDH: lipoic acid bound PDH, LA-KGDH: lipoic acid bound KGDH. (**E**) Representative SDH histoenzymatic activity staining in lumbar DRG at 5.5 weeks of age WT and *Pvalb* cKO mice. Scale bars, 100µm. (**F-G**) Heart cryosections (apex) from 9 weeks WT and MCK mutant mice[19] (**F**) and cerebellum cryosections from 13.5 weeks WT and *Pvalb* cKO mice (**G**) stained with Perl's DAB. Scale bars, 500µm.

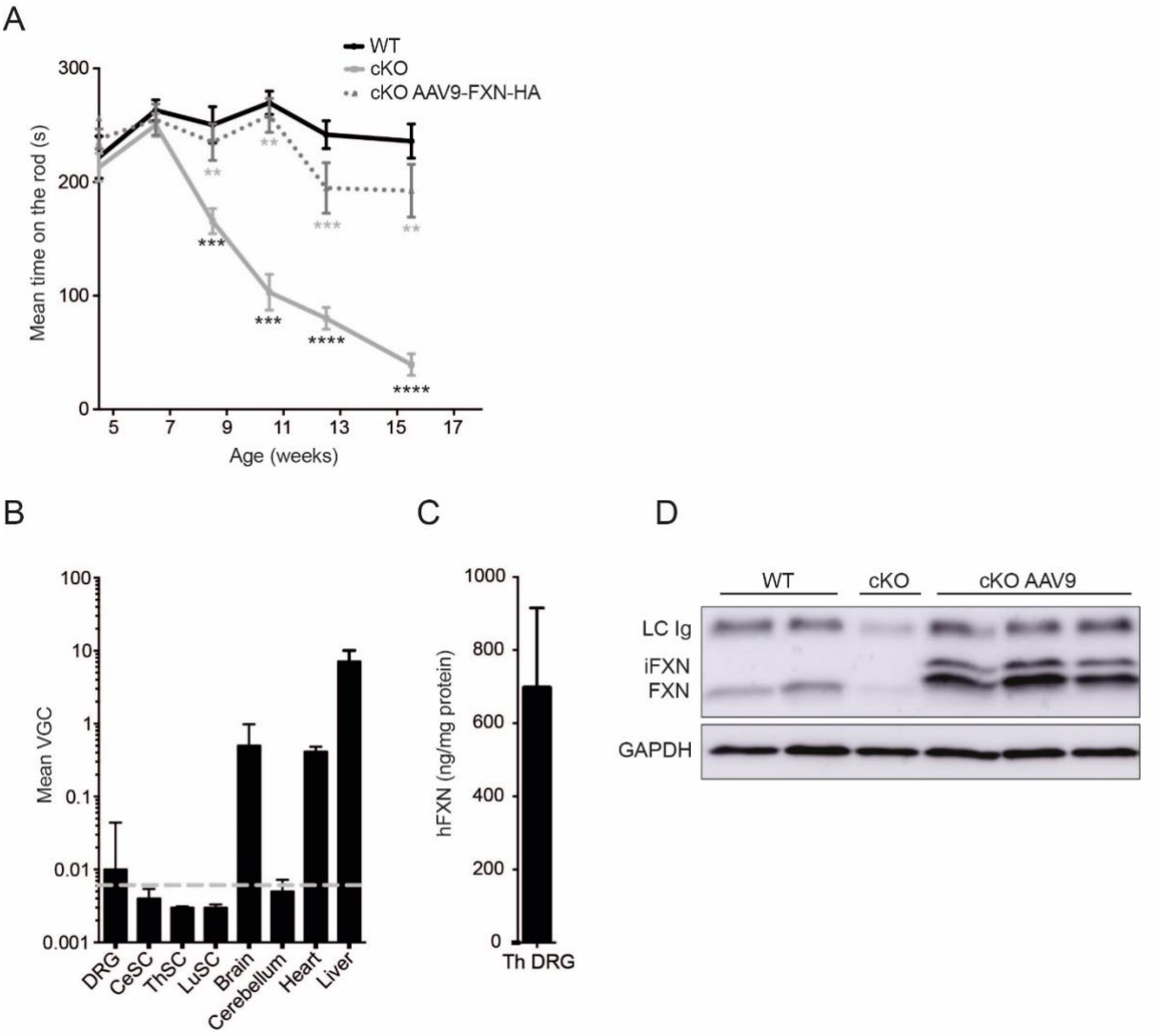

Figure S5: Early symptomatic treatment in *Pvalb* cKO animals

(**A**) Motor performances after early symptomatic treatment on the rotarod N= 11 WT, N= 9 *Pvalb* cKO and N= 9 *Pvalb* cKOAAV. (**B**) Biodistribution of AAV9-CAG-hFXN-HA after IV delivery and (**C**) quantification of human frataxin expression in thoracic DRG by ELISA, N= 3 animals per group. (**D**) Expression of mouse and human frataxin protein in thoracic DRG from WT, *Pvalb* cKO and *Pvalb* cKOAAV mice at 10.5weeks of age. LC Ig: Immunoglobulins light chains; iFXN: intermediate frataxin; FXN: mature frataxin. Data are represented as mean +/- SEM. *p<0.05; **p<0.01; ***p<0.001; ****p<0.0001.

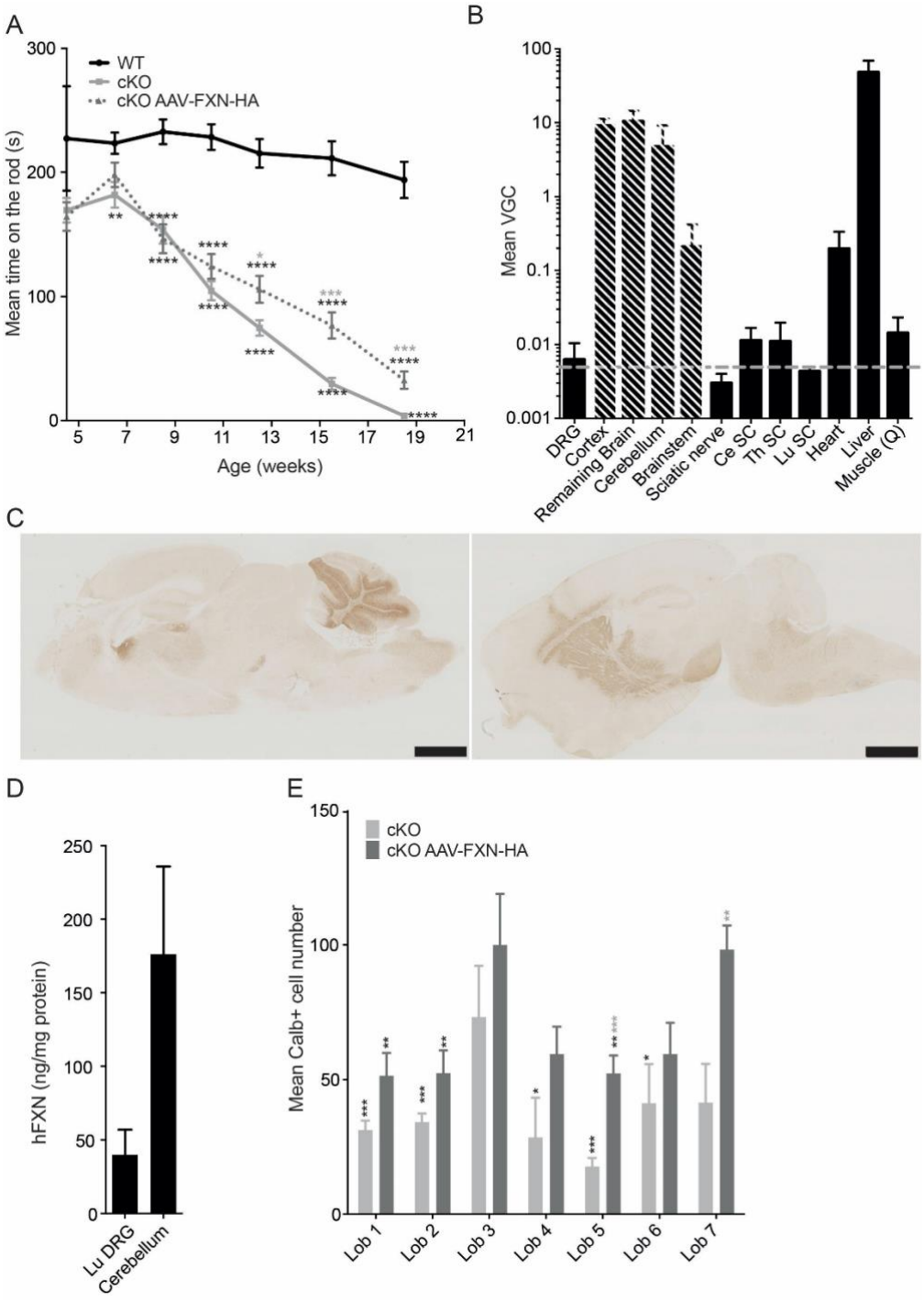

Figure S6: Late symptomatic treatment in *Pvalb* cKO animals

(A) Motor performances after late symptomatic treatment on the rotarod N= 26 WT, N= 29 *Pvalb* cKO and N= 32 *Pvalb* cKOAAV. (**B**) Biodistribution of AAV-CAG-hFXN-HA after IV and IC delivery, dashed bars correspond to VGC coming mainly from AAVrh10 IC delivery, N= 3. (**C**) Immunostaining for Frataxin HA expression in brain, Scale bars, 100µm. (**D**) Quantification of human frataxin (hFXN) expression in lumbar DRG and cerebellum, N= 3 animals per group. (**E**) Mean Purkinje cell number in different lobules of the cerebellum of WT, *Pvalb* cKO treated and untreated mice, N= 6 mice analyzed per group. Black stars correspond to p-value versus WT and grey stars versus KO. Data are represented as mean +/- SEM. *p<0.05; **p<0.01; ***p<0.001; ****p<0.0001.

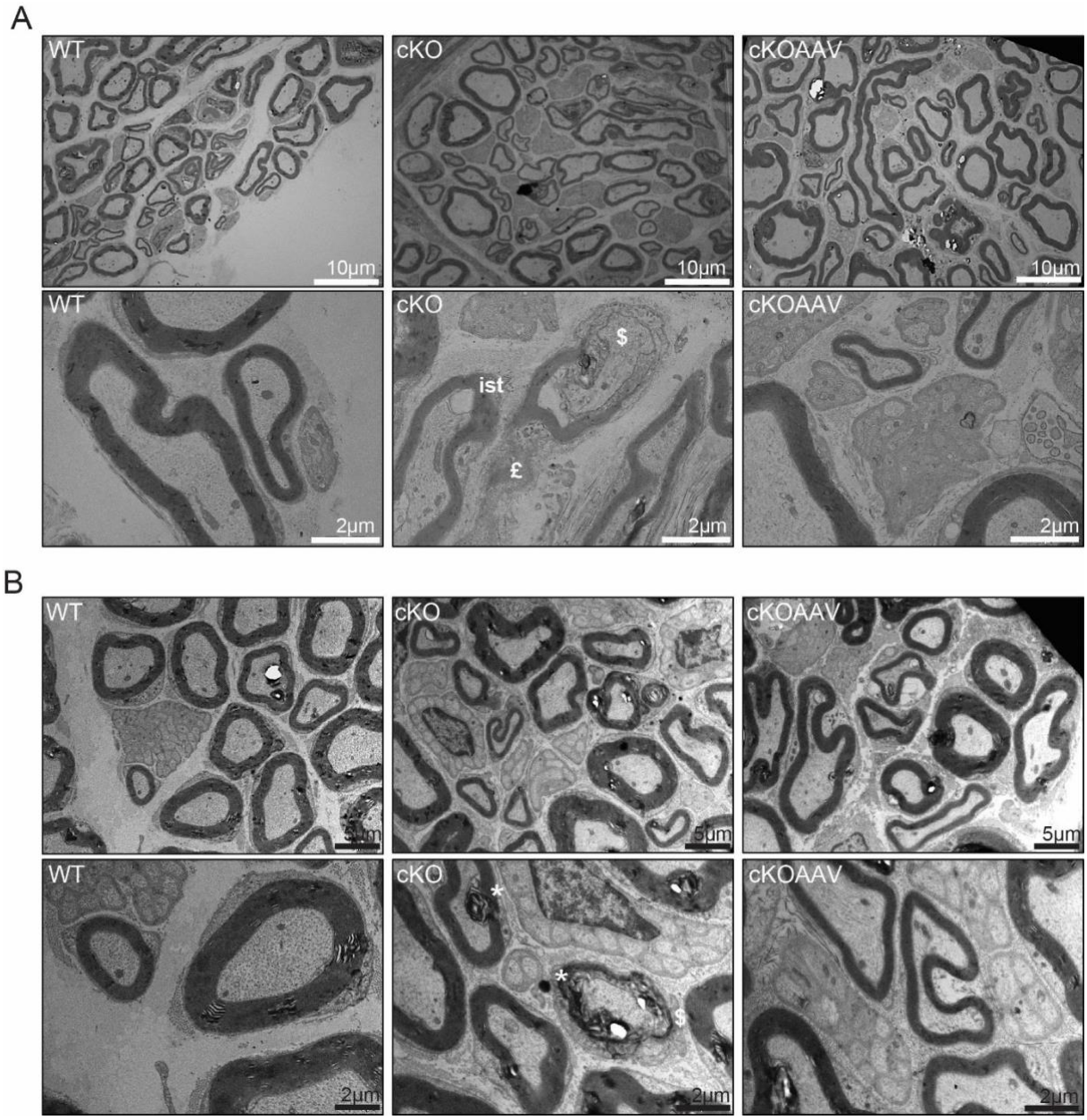

Figure S7: **Regeneration process in the sciatic nerve of *Pvalb* cKO animals treated at 7.5 weeks of age.** Ultrathin sections of sciatic nerves of WT, *Pvalb* cKO untreated and treated at 7.5 weeks and analyzed 1 week (**A**) or 2 weeks (**B**) post injection; ist: inner swelling tongue; £: fibrosis; $: degeneration; * : myelin debris. Scale bars, indicated sizes.

Table S1: Individual EMG data on characterization cohort

Mice	Sex	Genotype	6.5 weeks		8.5 weeks		10.5 weeks		12.5 weeks	
			Amp M wave	**Amp H wave**	Amp M wave	**Amp H wave**	Amp M wave	**Amp H wave**	Amp M wave	**Amp H wave**
84	F	WT	3,9	**0,4**	9,6	**0,5**	8,4	**0,6**	6	**0,9**
86	F	WT	6,9	**0,7**	3,9	**0,5**	6,8	**1,2**	5,7	**0,6**
87	F	WT	7	**1,3**	5	**1**	3,9	**0,4**	17,7	**1,5**
97	M	WT	11,8	**2,9**	9,2	**0,8**	11,7	**0,9**	4,8	**0,7**
98	M	WT	10,9	**1,1**	8,1	**0,6**	8,8	**0,6**	4,6	**0,7**
110	M	WT	4	**0,4**	5,3	**1**	7,7	**0,6**	7,2	**0,4**
88	F	KO	8,6	**0**	9,1	**0**	10,4	**0**	3,8	**0**
89	F	KO	8,4	**0,9**	3,7	**0**	4,2	**0**	12,3	**0**
90	F	KO	7,7	**1,2**	4	**0**	4,4	**0**	10,5	**0**
93	M	KO	7,5	**0,1**	5,4	**0**	5,4	**0**	3,5	**0**
95	M	KO	15,4	**1**	6,3	**0**	5,9	**0**	15	**0**
109	M	KO	4	**0**	12,3	**0**	4	**0**	11,2	**0**
111	M	KO	6	**0,3**	18,7	**0**	13,3	**0**	7,3	**0**

Table S2: ELISA assay on FXN expression

	Mean quantity of frataxin per mg of protein +/- SEM		% of FXN quantity in *Pvalb* cKO mice compare to WT		FXN level decrease in *Pvalb* cKO
	WT	***Pvalb* cKO**	**WT**	***Pvalb* cKO**	
Ce DRG	12.2 +/- 0.6 ng	2.1 +/- 0.2 ng	100%	17.2%	82.80%
Th DRG	25.8 +/- 2.3 ng	7.2 +/- 0.4 ng	100%	27.9%	72.10%
Lu DRG	25.6 +/- 2.1 ng	7.0 +/- 0.6 ng	100%	27.3%	72.70%
Cerebellum	27.8 +/- 0.7 ng	4.6 +/- 0.2 ng	100%	16.5%	83.50%

Table S3: Calculation for determining percentage of FXN expression

	Experimental value	Expected value		Experimental value		Difference between expected value and experimental value	
	WT ($Fxn^{+/L3}$)	Heterozygous without *Pvalb* Cre expression ($Fxn^{L3/L-}$)		*Pvalb* cKO ($Fxn^{L3/L-}$ *Pvalb* Cre)			
	Measured value (in ng of frataxin / mg prot)	Value WT/2 (in ng / mg prot)	Considered % of frataxin in heterozygous tissues	Quantity of frataxin expressed by the tissues (in ng / mg prot)	Equivalent % (vs heterozygotes) expressed by the tissues	Difference between expected value and experimental value (in ng / mg prot)	Equivalent % (vs heterozygotes) expressed by Cre positive cells
Ce DRG	12.2	6.1	100%	2.1	34.4 %	4	65.6 %
Th DRG	25.8	12.9	100%	7.2	55.8 %	5.7	44.2 %
Lu DRG	25.6	12.8	100%	7.0	54.7 %	5.8	45.3%
Cerebellum	27.8	13.9	100%	4.6	33.1 %	9.3	67%

Table S4: Individual EMG data on early-symptomatic treatment cohort

Mice	Sex	Genotype	6.5 weeks		8.5 weeks		10.5weeks		12.5weeks		15.5weeks	
			Amp M wave	**Amp H wave**	Amp M wave	**Amp H wave**	Amp M wave	**Amp H wave**	Amp M wave	**Amp H wave**	Amp M wave	**Amp H wave**
32	F	Fxn +/L3	6,4	**1,6**	7	**1,1**	5,3	**0,9**	8,4	**1**	ND	**ND**
145	F	Fxn +/L3	3,8	**0,4**	14,5	**0,4**	5,4	**1,1**	5,2	**0,3**	5,5	**1**
146	F	Fxn +/L3	7,6	**1,6**	7,3	**1,4**	7	**0,3**	10,4	**2,1**	7,7	**1**
141	F	Fxn +/L3	3	**0,2**	10,5	**0,7**	10	**0,6**	16,2	**0,7**	6,3	**0,6**
158	M	Fxn L3/L-	5,7	**0,2**	8,4	**1,9**	6,8	**0,5**	4,9	**0,3**	10,3	**0,6**
155	M	Fxn +/L3	4	**0,3**	7,7	**0,6**	11,3	**0,5**	3,4	**0,5**	15,5	**0,3**
152	M	Fxn +/L3 Pvalb +	7	**0,8**	14,5	**0,2**	10,9	**0,7**	4,9	**0,3**	2,9	**0,2**
5	F	Fxn L3/L-	5,1	**1**	13,2	**0,5**	14,8	**3,1**	13,3	**0,4**	ND	**ND**
7	F	Fxn L3/L-	11	**0,4**	10,5	**2,3**	11,1	**0,6**	8,1	**1,2**	ND	**ND**
16	M	Fxn +/L3	2,7	**0**	14,1	**1,1**	5,8	**0,4**	11,5	**0,3**	11,1	**1,2**
25	M	Fxn +/L3	3,9	**0,6**	4,5	**0,6**	6,7	**1,7**	12,2	**0,6**	5,8	**0,8**
30	F	Fxn L3/L- Pvalb +	15,4	**1**	9,6	**0,6**	15,5	**0**	5,4	**0**	ND	**ND**
34	M	Fxn L3/L- Pvalb +	8,1	**0,5**	7,6	**0,1**	4,9	**0**	9,9	**0**	ND	**ND**
151	F	Fxn L3/L- Pvalb +	6,2	**0**	5,8	**0**	5,7	**0**	2,6	**0**	16,1	**0**
143	F	Fxn L3/L- Pvalb +	17,5	**0**	10	**0,4**	11,7	**0**	10,2	**0**	6,4	**0**
153	M	Fxn L3/L- Pvalb +	10	**0**	1,5	**0**	1,6	**0**	7,1	**0**	10,6	**0**
154	M	Fxn L3/L- Pvalb +	12	**0,3**	8	**0**	7,2	**0**	7	**0**	4,2	**0**
15	M	Fxn L3/L- Pvalb +	9,8	**0,5**	11,1	**0**	12,5	**0**	12,5	**0**	6,2	**0**
37	M	Fxn L3/L- Pvalb +	10	**0**	3,9	**0**	3,6	**0**	ND	**ND**	12,7	**0**
58	F	Fxn L3/L- Pvalb +	9,7	**1,2**	12,9	**0,6**	11,6	**0,7**	ND	**ND**	5,4	**0**
142	F	Fxn L3/L- Pvalb + AAV	11,5	**0,9**	9,3	**0,5**	7,4	**0,4**	12,5	**2,9**	3	**0,7**
149	F	Fxn L3/L- Pvalb + AAV	4,8	**1,1**	8,8	**0,4**	6,1	**0,5**	10,4	**1,1**	13,3	**0,7**
156	M	Fxn L3/L- Pvalb + AAV	9,1	**0,6**	4	**0,2**	9,4	**0,9**	4,4	**0,4**	7,5	1
157	M	Fxn L3/L- Pvalb + AAV	4,9	**0,7**	5	**1,3**	3	**0,3**	5	**0,2**	6,6	0,1
159	M	Fxn L3/L- Pvalb + AAV	6,3	**0,8**	8,7	**2,2**	6,4	**0,6**	10,3	**0,7**	4,6	0,6
6	F	Fxn L3/L- Pvalb + AAV	7,4	**0,7**	10,1	**1,2**	12	**3,2**	6,4	**0,6**	ND	ND
8	F	Fxn L3/L- Pvalb + AAV	8,7	**0,6**	11	**0,9**	13,3	**0,6**	9,7	**0,8**	ND	ND
39	M	Fxn L3/L- Pvalb + AAV	2,1	**0,4**	8,2	**2,5**	4,5	**0,9**	ND	ND	4,3	1,1
62	M	Fxn L3/L- Pvalb + AAV	11,6	1,2	9	**2**	14,1	**1,2**	ND	ND	16,1	1

ND: not determined because mouse would not sleep

Table S5: Individual EMG data on post-symptomatic treatment cohort

Mice	Sex	Genotype	6.5 weeks		8.5 weeks		10.5weeks		12.5weeks		15.5weeks		19.5weeks	
			Amp M wave	**Amp H wave**	Amp M wave	**Amp H wave**	Amp M wave	**Amp H wave**	Amp M wave	**Amp H wave**	Amp M wave	**Amp H wave**	Amp M wave	**Amp H wave**
75	M	Fxn +/L3	12,2	**1,2**	6	**1,8**	6,1	**0,3**	11,9	**0,6**			4,5	**0,3**
61	F	Fxn +/L3 Pvalb+	6,9	**0,3**	2	**0,3**	4,8	**0,8**	7	**0,2**	4,1	**0,5**		
78	F	Fxn +/L3	5,8	**0,6**	16,9	**0,7**	8,9	**1,9**	4,7	**0,1**			7,1	**0,4**
83	F	Fxn +/L3	5,7	**0,2**	4,2	**0,3**	14,2	**0,7**	7,6	**0,4**			6,3	**0,5**
84	F	Fxn +/L3	8,2	**1,3**	9,7	**0,6**	5,6	**0,5**	6,2	**1,1**			5,9	**0,6**
103	F	Fxn +/L3	7,2	**2**	13,8	**0,7**	11,5	**1**	9,2	**0,8**	13,3	**1,2**	13,3	**0,5**
108	F	Fxn +/L3	15,6	**0,4**	11,2	**1,1**	4	**0**	3,7	**0,4**	5,6	**0,3**	11,7	**0,5**
112	M	Fxn +/L3	11,6	**0,4**	16,8	**1,4**	9,8	**1,9**	3,7	**1,1**	5,5	**0,1**	5,5	**0,2**
113	M	Fxn +/L3	11,8	**0,4**	5,3	**1,3**	7,4	**0,5**	2,5	**0,3**	4,9	**0,4**	5,1	**0,3**
85	F	Fxn +/L3	2,3	**0,6**	ND	**ND**	8,1	**1,2**	ND	**ND**	7	**0,7**		
143	F	Fxn +/L3	ND	**ND**	ND	**ND**	8	**1,6**	6,5	**0,8**	11,2	**0,8**		
145	M	Fxn +/L3	ND	**ND**	ND	**ND**	6,7	**1,1**	7,8	**0,7**	7,9	**0,1**		
94	F	Fxn +/L3	4,1	**0,3**	2,5	**0,1**	3	**0,5**	5,4	**0,3**	7,4	**1**		
101	M	Fxn +/L3	ND	**ND**	2,6	**0,3**	1,2	**0,3**	4,3	**0,4**	1,7	**0,3**		
109	F	Fxn +/L3 Pvalb +	5,9	**1,2**	9,2	**1,2**	2,6	**1,3**	7,7	**0,9**	5,4	**1,2**		
115	M	Fxn +/L3 Pvalb +	1,9	**0,3**	3	**0,4**	4,9	**0,2**	3,4	**0,5**	4,5	**0,9**		
12	M	Fxn +/L3 Pvalb+	4,4	**0,7**	4,2	**0,3**	4,6	**0,6**	5,2	**0,7**	5,7	**0,5**		
66	F	Fxn +/L3 Pvalb+	5,9	**0,4**	4,3	**0,7**	6,5	**0,3**	3,4	**0,9**	5,7	**0,5**		
68	F	Fxn +/L3 Pvalb+	1,2	**0,4**	6	**0,9**	6,7	**1**	3,2	**0,3**	9,3	**0,4**		
69	F	Fxn +/L3 Pvalb+	3,2	**0,4**	5,2	**0,6**	3,3	**0,3**	4,9	**0,4**	6,9	**0,8**		
71	F	Fxn +/L3 Pvalb+	3,2	**0,5**	5,3	**0,7**	4	**0,6**	4,2	**0,8**	6,6	**0,7**		
52	M	Fxn +/L3 Pvalb+	6,6	**0,3**	7,2	**0,6**	4	**0,4**	ND	**ND**	10,7	**0,8**		
53	M	Fxn +/L3 Pvalb+	4,9	**0,4**	5,7	**0,2**	6,1	**0,9**	ND	**ND**	4,3	**0,6**		
57	F	Fxn +/L3 Pvalb+	ND	**ND**	3,1	**0,3**	7,7	**1,8**	2,5	**0,4**	4,6	**0,8**		
162	F	Fxn +/L3 Pvalb+	4,7	**0,2**	13,2	**0,7**	4,1	**1,1**	3	**0,6**	8,2	**1,3**		
79	M	Fxn +/L3 Pvalb+	4,1	**0,6**	5,3	**0,3**	3	**0,3**	4,8	**0,8**	3,7	**0,3**		
76	M	Fxn L3/L- Pvalb+	7,2	**0**	3,5	**0**	6	**0**	4,7	**0**			15,1	**0**
77	M	Fxn L3/L- Pvalb+	8,5	**0**	5,4	**0**	4,9	**0**	6,6	**0**			4,4	**0**
71	F	Fxn L3/L- Pvalb+	9,9	**0,9**	15,5	**0**	14,9	**0**	3,9	**0**			11,6	**0**
74	F	Fxn L3/L- Pvalb+	5,4	**0,4**	8,9	**0**	6,6	**0**	14,8	**0**			7,1	**0**
79	F	Fxn L3/L- Pvalb+	8,2	**0,4**	7,9	**0**	4,4	**0**	9,7	**0**			8,1	**0**
117	F	Fxn L3/L- Pvalb+	6,9	**0**	4,1	**0**	7,6	**0**	11,6	**0**			5,7	**0**
118	F	Fxn L3/L- Pvalb+	2,1	**0**	2,2	**0**	5	**0**	4,9	**0**	7	**0**	2,3	**0**
124	F	Fxn L3/L- Pvalb+	6,1	**0**	4,4	**0**	7,7	**0**	14,7	**0**	7,8	**0**	9,6	**0**
161	F	Fxn L3/L- Pvalb+	3,5	**0**	3,3	**0**	7	**0**	4,8	**0**	6,4	**0**		
88	M	Fxn L3/L- Pvalb+	3,1	**0,2**	1,1	**0**	2,5	**0**	4,3	**0**	3,2	**0**		
154	M	Fxn L3/L- Pvalb+	ND	**ND**	ND	**ND**	10,6	**0**	2	**0**	4,5	**0**		
144	F	Fxn L3/L- Pvalb+	ND	**ND**	ND	**ND**	5,3	**0**	0,9	**0**	5,4	**0**		
159	M	Fxn L3/L- Pvalb+	ND	**ND**	ND	**ND**	2,3	**0**	10,1	**0**	10,7	**0**		
98	F	Fxn L3/L- Pvalb+	2,4	**0,7**	4,2	**0**	6,5	**0**	8,7	**0,1**	2,3	**0**		
107	F	Fxn L3/L- Pvalb+	2,9	**0,1**	3,2	**0**	1,2	**0**	3,1	**0**	5,1	**0**		
122	F	Fxn L3/L- Pvalb+	1,9	**0,2**	7,8	**0**	1,8	**0**	11,4	**0**	5,2	**0**		
124	M	Fxn L3/L- Pvalb+	4	**0**	6,1	**0**	2,8	**0**	7,2	**0,1**	3,3	**0**		
184	F	Fxn L3/L- Pvalb+	10,2	**0,5**	3,1	**0**	5,7	**0**	5,2	**0**	9	**0**		
188	M	Fxn L3/L- Pvalb+	6,7	**0**	5,9	**0**	3,4	**0**	5,8	**0**	8,6	**0**		
179	M	Fxn L3/L- Pvalb+	6,1	**0,7**	5,5	**0**	2	**0**	4,9	**0**	5,2	**0**		
160	F	Fxn L3/L- Pvalb+	1,4	**0**	2,2	**0**	10,4	**0**	7,3	**0**	6,5	**0**		
163	M	Fxn L3/L- Pvalb+	4	**0**	7,6	**0**	9,5	**0**	3,5	**0**	6,1	**0**		
14	M	Fxn L3/L- Pvalb+	3,7	**0**	6	**0**	4,8	**0**	7,2	**0**	6,5	**0**		
183	F	Fxn L3/L- Pvalb+	4,1	**0,3**	2,6	**0**	7,5	**0**	4,9	**0**	3,7	**0**		
73	F	Fxn L3/L- Pvalb+	4,2	**0,5**	14	**0**	6,3	**0**	4,9	**0**	11,4	**0**		
77	M	Fxn L3/L- Pvalb+	ND	**ND**	2	**0**	3,8	**0**	11,2	**0**	3	**0**		
49	F	Fxn L3/L- Pvalb+	4	**0**	10,2	**0**	10,4	**0**	10,7	**0**	5,2	**0**		
58	F	Fxn L3/L- Pvalb+	4,1	**0**	4,7	**0**	8,4	**0**	11	**0**	2,9	**0**		
64	M	Fxn L3/L- Pvalb+	4,5	**0**	4,5	**0**	8,3	**0**	1,2	**0**	5	**0**		
82	F	Fxn L3/L- Pvalb+ AAV	9,5	**0,9**	5,1	**1,4**	6,1	**0,5**	12	**1**			9,6	**0,9**
85	F	Fxn L3/L- Pvalb+ AAV	2,5	**1,1**	5,5	**0,6**	6,7	**0,6**	2,9	**0,9**			4,2	**0,5**
88	M	Fxn L3/L- Pvalb+ AAV	7,1	**0**	7,1	**0,2**	7,2	**1,5**	6,4	**0,3**			6,7	**0,7**
105	F	Fxn L3/L- Pvalb+ AAV	3,3	**0**	5,9	**0,6**	5,7	**0**	7,4	**0,2**	6,6	**1**	7,7	**0,4**
106	F	Fxn L3/L- Pvalb+ AAV	11,1	**0,5**	2,7	**0,1**	2,5	**1**	6,2	**0,5**	8,7	**0,7**	6,3	**0,3**
110	F	Fxn L3/L- Pvalb+ AAV	8	**0,2**	9,9	**1,3**	6,3	**0,8**	1,4	**0,2**	6,3	**0,3**	5,8	**0,6**
125	M	Fxn L3/L- Pvalb+ AAV	9,9	**1,2**	5	**0,4**	8,4	**0,8**	10,9	**0,2**	11,7	**0,4**	4,4	**0,3**
127	M	Fxn L3/L- Pvalb+ AAV	4,2	**0**	10,5	**0,5**	5,8	**0,3**	7,2	**0,7**	4,6	**0,4**	8,8	**0,3**
128	M	Fxn L3/L- Pvalb+ AAV	2,8	**0**	7,4	**0,3**	11,6	**0,3**	7,9	**0,2**	2,7	**0,7**	5,1	**0,4**
137	F	Fxn L3/L- Pvalb+ AAV	5,3	**0**	4,8	**0**	6,7	**0**	5,4	**0**	10,6	**0**		
160	F	Fxn L3/L- Pvalb+ AAV	9,9	**0**	4,6	**0,5**	9,8	**0,8**	8,2	**0,4**	8,9	**1**		
149	M	Fxn L3/L- Pvalb+ AAV	ND	**ND**	ND	**ND**	5,9	**0,9**	6,4	**0,8**	14,1	**0,4**		
156	F	Fxn L3/L- Pvalb+ AAV	ND	**ND**	ND	**ND**	4,1	**1**	2	**0,6**	4,1	**0,1**		
160	M	Fxn L3/L- Pvalb+ AAV	ND	**ND**	ND	**ND**	2	**0**	3,6	**0,5**	8,6	**0,4**		
95	F	Fxn L3/L- Pvalb+ AAV	8	**0,3**	14,5	**0,5**	3,7	**0,3**	6,8	**0,2**	6,8	**0,4**		
96	M	Fxn L3/L- Pvalb+ AAV	2,7	**0**	10,7	**0,4**	4	**0,1**	7,9	**0,3**	3,1	**0,2**		
100	M	Fxn L3/L- Pvalb+ AAV	2,3	**0**	5,5	**0,2**	1,6	**0,5**	ND	**ND**	6,4	**0,6**		
106	F	Fxn L3/L- Pvalb+ AAV	ND	**ND**	10,4	**1,6**	5,8	**0,2**	7,3	**0**	ND	**ND**		
111	F	Fxn L3/L- Pvalb+ AAV	12,5	**0,5**	4,5	**0,3**	2,3	**0,2**	8,4	**0,3**	8,2	**0,8**		
118	M	Fxn L3/L- Pvalb+ AAV	6,3	**0,1**	9,7	**0,1**	8,7	**0,2**	5,6	**0,8**	3,7	**0,8**		
190	M	Fxn L3/L- Pvalb+ AAV	5,2	**0,3**	7,1	**0,7**	2,8	**0,4**	2,8	**0,2**	4,7	**0,3**		
178	F	Fxn L3/L- Pvalb+ AAV	2,5	**0,1**	4,4	**0,4**	5,7	**0,9**	2,2	**0,3**	ND	**ND**		
180	M	Fxn L3/L- Pvalb+ AAV	2,4	**0**	2,9	**0,4**	4,4	**0,2**	3,2	**0,3**	2,9	**0,3**		
174	F	Fxn L3/L- Pvalb+ AAV	10	**0**	5,4	**0,3**	6,5	**0,7**	3,2	**0,3**	5,1	**0,4**		
161	F	Fxn L3/L- Pvalb+ AAV	4,4	**0**	5,1	**0,3**	3,4	**0,6**	7,1	**0,5**	2,2	**0,8**		
164	M	Fxn L3/L- Pvalb+ AAV	0,5	**0**	7,2	**0,2**	3,3	**0,4**	3,7	**0,5**	5,1	**0,4**		
165	M	Fxn L3/L- Pvalb+ AAV	4,8	**0**	3,2	**0,3**	ND		7,4	**0,5**	4,8	**0,5**		
5	F	Fxn L3/L- Pvalb+ AAV	5,1	**0**	3,6	**1,3**	8,7	**0,4**	2,8	**0,6**	3,2	**0,4**		
181	F	Fxn L3/L- Pvalb+ AAV	3,2	**0,4**	5,8	**0,2**	2,7	**0,5**	4,5	**0,2**	3,2	**0,7**		
60	F	Fxn L3/L- Pvalb+ AAV	5,4	**0**	12	**0,7**	3,8	**0,6**	7,5	**0,4**	7,8	**0,5**		
50	M	Fxn L3/L- Pvalb+ AAV	5,4	**0**	9,3	**0,9**	7,6	**1**	3,3	**0,4**	5,6	**0,4**		
51	M	Fxn L3/L- Pvalb+ AAV	5,6	**0**	8,7	**0,6**	2	**0,4**	8,2	**0,5**	1,2	**0,5**		

ND: not determined because mouse would not sleep

Hatched: not measured

Table S6: Stereotaxic coordinates for injection

	Stereotaxic coordinates from the Bregma		
Injection site	Antero-posterior (AP)	Medio-lateral (ML)	Dorso-ventral (DV)
Striatum 1st injection site	+0.5mm	+2.2mm	-3.3mm
Striatum 2nd injection site	+0.5mm	-2.2mm	-3.3mm
White matter of the cerebellum	-6.48mm	0mm	-2.5mm

Table S7: List of antibodies used

	Antibodies	Application	Used Concentration	Species	Reference	Company
primary antibodies	Anti HA-TAG	IF	1:250	rabbit	C29F4	Cell Signalling Technology
	Anti Calbindin	IF	1:500	rabbit	CB38-A	Swant swiss Antibodies
	Anti MBP	IF	1:200	mouse	SMI-94	Calbiochem
	Anti NF-200	IF	1:200	chicken	ab4680	Abcam
	Anti TfR1	IF	1:500	rabbit	ab84036	Abcam
	Anti GFAP	IF	1:500	guinea pig	173004	Synaptic systems
	Anti frataxin polyclonal	WB	1:1,000	rabbit	R1250	IGBMC
	Anti frataxin monoclonal	WB	1:1,000	mouse	4F9	IGBMC
	Anti GAPDH	WB	1:20,000	mouse		IGBMC
	Anti lipoic acid	WB	1:5,000	rabbit	437695	Calbiochem
secondary antibodies	Biotinylated Anti-Rabbit IgG	IF	1:500	goat	BA-1000	Vector laboratories
	Anti-Rabbit IgG 488	IF	1:1,000	goat	A-11008	Life Technologies
	Anti-Mouse IgG 594	IF	1:1,000	goat	A-11005	Life Technologies
	Anti-Chicken IgG 488	IF	1:1,000	donkey	703-545-155	Interchim SA
	Anti-Rabbit IgG 594	IF	1:1,000	goat	A-11037	Life Technologies
	Anti-Guinea pig IgG 488	IF	1:1,000	goat	A-11073	Life Technologies
	Peroxydase Anti-mouse IgG	WB	1:5,000	goat	115-035-046	Jackson ImmunoResearch
	Peroxydase Anti-rabbit IgG	WB	1:5,000	goat	115-035-146	Jackson ImmunoResearch

Supplemental results:

Validation of expression of Pvalb-Cre transgene

As endogenous parvalbumin expression is not restricted to the proprioceptive sensory neurons (http://mouse.brain-map.org/gene/show/19056) and behavioral analysis clearly showed that the *Pvalb* cKO develop a cerebellar/cortical phenotype, in addition to the sensory neuropathy, we evaluated the tissue specificity and the temporal expression of the *Pvalb-Cre* transgene in *Pvalb*$^{tm1(Cre)Arbr/J}$ transgenics using the ROSA26/LacZ reporter stain. LacZ expression was analyzed at several time points: E14.5, E17.5, P8, P40 and 21.5 weeks. While no LacZ staining was detected at E14.5, positive LacZ in DRG was observed at E17.5 (Figure S2A-B). By p8, approximately 15% of DRG neurons were positive for LacZ (Figure S2C) and in a similar manner in cervical, thoracic and lumbar DRG (Figure S2D-F respectively). Therefore, the *Pvalb*-Cre expression in the DRG starts between E14 and E17.5 as described previously[21] and is fully expressed by p8. No LacZ staining was detect in peripheral nerves. In the central nervous sytem, no LacZ staining was seen at p8. At p40, LacZ staining was specifically detected in Purkinje cells (Figure S2G-H). At 21.5 weeks, positive LacZ staining was detected in the interposed nucleus, a deep central grey nucleus (Figure S2G), in interneurons in the cortex (Figure S2I), few positive cells in the hippocampus (Figure S2J), strong staining in the majority of the red nucleus (Figure S2K), superior olivary complex and the pontine grey (Figure S2L). No LacZ positive staining was detected in any peripheral tissues at any time point analyzed.

Quantification of frataxin expression

WT animals are +/L3 for the frataxin allele, meaning that they express 100% of frataxin in all tissues. *Pvalb* cKO animals are heterozygous for the frataxin locus (*Fxn*$^{L3/L-}$) in all cells except the cells expressing the Cre recombinase which are homozygous for the depletion (*Fxn*$^{L-/L-}$). Thus, we expect 50% of frataxin expression in the heterozygous cells (*Fxn*$^{L3/L-}$) and no expression in the knocked-out cells (*Fxn*$^{L-/L-}$). By measuring frataxin levels in the heterogeneous tissues of interest (DRG and cerebellum), we can determine the amount/percentage of frataxin expressed by the Cre positive cells (Expected values in heterozygotes animals – experimental values in *Pvalb* cKO animals).

Example for calculation in lumbar DRG (other tissues are in table S2 and S3):

25.6ng of frataxin per mg of protein were experimentally measured in WT lumbar DRG. Therefore, we expect 12.8 ng of frataxin per mg of protein in heterozygous lumbar DRG without *Pvalb*-Cre expression (considered as 100%). Upon *Pvalb*-Cre expression 7.0 ng of frataxin were measured (~55%). Thus, the Cre positive cells express 5.8 ng of frataxin per mg of protein (12.8 – 7.0 = 5.8), approximately 45%.